1 **MYC Serine 62 phosphorylation promotes its binding to DNA double strand**

2 **breaks to facilitate repair and cell survival under genotoxic stress.**

3

4 Gabriel M. Cohn[1], Colin J. Daniel[1], Jennifer R. Eng[1], Xiao-Xin Sun[1], Carl Pelz[1,2], Koei

5 Chin[3,4], Alexander Smith[2], Charles D. Lopez[2,5,6], Jonathan R. Brody[2,6,7,8], Mu-shui Dai[1],

6 Rosalie C. Sears[1,2,6]

7

8 [1]Department of Molecular and Medical Genetics, School of Medicine, Oregon Health

9 and Science University, Portland, OR, USA

10 [2]Brenden-Colson Center for Pancreatic Care, Oregon Health and Science University,

11 Portland, OR, USA

12 [3]Center for Early Detection Advanced Research, Oregon Health and Science University,

13 Portland, OR, USA

14 [4]Department of Biomedical Engineering, Oregon Health and Science University,

15 Portland, OR, USA

16 [5]Department of Hematology and Oncology, Oregon Health and Science University,

17 Portland, OR, USA

18 [6]Knight Cancer Institute, Oregon Health and Science University, Portland, OR, USA

19 [7]Department of Surgery, Oregon Health and Science University, Portland, OR, USA

20 [8]Department of Cell, Developmental and Cancer Biology, Oregon Health and Science

21 University, Portland, OR, USA

22

23

24 Corresponding Author:

25 Rosalie C. Sears

26 Oregon Health & Science University

27 searsr@ohsu.edu

28

Abstract

Genomic instability is a hallmark of cancer, driving oncogenic mutations that enhance tumor aggressiveness and drug resistance. MYC, a master transcription factor that is deregulated in nearly all human tumors, paradoxically induces replication stress and associated DNA damage while also increasing expression of DNA repair factors and mediating resistance to DNA-damaging therapies. Emerging evidence supports a non-transcriptional role for MYC in preserving genomic integrity at sites of active transcription and protecting stalled replication forks under stress. Understanding how MYC's genotoxic and genoprotective functions diverge may reveal new therapeutic strategies for MYC-driven cancers. Here, we identify a non-canonical role of MYC in DNA damage response (DDR) through its direct association with DNA breaks. We show that phosphorylation at serine 62 (pS62-MYC) is crucial for the efficient recruitment of MYC to damage sites, its interaction with repair factors BRCA1 and RAD51, and effective DNA repair to support cell survival under stress. Mass spectrometry analysis with MYC-BioID2 during replication stress reveals a shift in MYC's interactome, maintaining DDR associations while losing transcriptional regulators. These findings establish pS62-MYC as a key regulator of genomic stability and a potential therapeutic target in cancers.

Introduction

53   MYC is a master transcriptional regulator that impacts all cellular pathways

54   involved in proliferation, differentiation, and response to cellular signals (Fernandez,

55   Frank et al. 2003, Chen, Liu et al. 2018). Due to its participation in anabolic and stress-

56   responsive biology, MYC deregulation is found in virtually all human cancers, is

57   prognostic for patient survival, and is often responsible for chemotherapy

58   resistance(Dang 2012, Gabay, Li et al. 2014, Stine, Walton et al. 2015, Kumari, Folk et

59   al. 2017). To prevent MYC's oncogenic effect in normal cells, MYC protein abundance

60   and activity is tightly regulated with a half-life of about 15-30 minutes under

61   physiological conditions(Hann and Eisenman 1984). MYC's stability is primarily

62   regulated through sequential phosphorylation events within MYC's transactivation

63   domain, Thr58 (pT58-MYC) and Ser62 (pS62-MYC) which impact its degradation

64   through the ubiquitin-proteosome system(Sears, Nuckolls et al. 2000, Welcker, Orian et

65   al. 2004, Sun, Li et al. 2021). Upon cell growth stimulation, MYC becomes transiently

66   stabilized by RAS-induced and/or cyclin-dependent kinase-mediated phosphorylation at

67   Ser62 resulting in increased MYC stability and activity(Lutterbach and Hann 1994,

68   Farrell, Pelz et al. 2013). To trigger MYC's degradation, subsequent phosphorylation at

69   Thr58 by GSK3 or BRD4 initiates MYC's engagement with the ubiquitin-proteosome

70   system (Gregory, Qi et al. 2003, Devaiah, Mu et al. 2020).

71   Mechanistically, MYC canonically functions as a transcription factor that enables

72   potent transcriptional amplification, intensifying the recruitment and assembly of multiple

73   protein complexes at each stage of transcription(Das, Lewis et al. 2023). MYC-driven

74   transcriptional amplification is accompanied by genomic burdens such as increased

3

75   torsional stress, R-loop formation, Transcriptional-Replication Conflicts (TRCs), among

76   others(Jha, Kouzine et al. 2023). To mitigate this increase in genomic stress, emerging

77   and non-canonical functions of MYC have recently been described. Along with recruiting

78   transcriptional machinery to active promoters, MYC nucleates a "topoisome" complex

79   between topoisomerase 1 & 2 to relieve DNA torsional stress produced by the elevated

80   transcription(Das, Kuzin et al. 2022). MYC has also been shown to facilitate the transfer

81   of polymerase associated factor 1c (PAF1c) to stalled RNA polymerase, activating

82   several chromatin modifying complexes and DNA repair to ensure high fidelity

83   elongation(Endres, Solvie et al. 2021). In response to a variety of cellular stressors

84   including transcriptional stress, replication stress, and proteolytic stress, MYC proteins

85   have been described to multimerize and protect replication-fork stability, decrease R-

86   loop formation, and terminate transcription, all to protect genomic stability in the

87   presence of stress(Papadopoulos, Solvie et al. 2022, Solvie, Baluapuri et al. 2022).

88   Accompanying these MYC multimers were DNA maintenance proteins which aligns with

89   previous findings that the neuronal MYC paralog, MYCN, and MYC are capable of

90   recruiting critical components of DNA repair such as BRCA1, the TRRAP-containing

91   NuA4 complex, and the p400 helicase to active promoters(Frank, Parisi et al. 2003,

92   Tworkowski, Chakraborty et al. 2008, Kim, Woo et al. 2010, Herold, Kalb et al. 2019,

93   Papadopoulos, Solvie et al. 2022). Although these studies have highlighted emerging

94   roles of MYC in safeguarding the genome under cellular stress, a direct role for MYC in

95   mediating DNA repair has not been explored.

96   In this study, we investigated a direct role of MYC in DNA repair in cancer cells

97   with a focus on pancreatic ductal adenocarcinoma (PDAC). Our previous research

98   demonstrated that MYC pathway activity is high in a subset of patients with aggressive,

99   liver metastatic PDAC, characterized by elevated replication stress and DNA repair

100   signatures(Link, Eng et al. 2025). We performed further analyses and confirmed a

101   strong correlation between MYC and the tumor's response to genomic instability, both at

102   the transcriptional and tissue levels. To investigate the cellular mechanisms behind this

103   strong correlation, we employed a DNA double-strand break (DSBs)-specific proximity

104   ligation assay to discover that MYC associates with DSBs and that genomic stress

105   enhances MYC's association with DSBs as well as repair proteins such as BRCA1 and

106   RAD51. Furthermore, using a MYC-BioID2 proximity-dependent proteomic approach,

107   we observed a shift in MYC's interactome under replication stress, marked by a notable

108   enrichment of DNA repair machinery. Mechanistically, we discovered that MYC's

109   association with DSBs is dependent on the phosphorylation at serine 62 (pS62-MYC).

110   Blocking this phosphorylation with a phosphorylation-deficient MYC mutant (S62A-

111   MYC) disrupts BRCA1 and RAD51 recruitment to DSBs, resulting in a reduction in DNA

112   repair and overall cell survival. Together, our findings reveal a novel direct role for MYC

113   in DNA damage repair, offering new insights into MYC's involvement in genome

114   maintenance that could be leveraged for new therapeutic strategies.

Results

MYC Activity Positively Correlates with Genomic stress, DNA repair and Poor Patient Survival in PDAC

Our recent study demonstrated that pancreatic ductal adenocarcinoma (PDAC) patients with tumors exhibiting higher molecular signatures of tolerance to replication stress are more likely to develop liver metastasis and experience poorer overall survival(Link, Eng et al. 2025). Furthermore, this study demonstrated that elevated MYC activity was associated with a tumor survival advantage under conditions of high replication stress and DNA damage. To explore this dataset of 218 primary tumors and 71 metastases further, we generated a replication stress gene set based on the intersection between known cell cycle, check point, and DNA replication genes. We found a significant positive correlation between this replication stress signature score and the hallmark MYC-V1 target pathway score (Figure 1A). Since tumor cells experiencing high proliferation and transcriptional activity are often deficient in biosynthetic activity, they face stalled and collapsed replication forks leading to DSBs and genomic damage (Vesela, Chroma et al. 2017, Dreyer, Upstill-Goddard et al. 2021). In agreement with the replication stress signature, elevated hallmark MYC-V1 targets pathway activity significantly positively correlated with the hallmark DNA repair pathway score in our patient PDAC tumor samples, suggestive of MYC's emerging non-canonical function involved in maintaining genomic integrity (Figure 1B). We then stratified our PDAC tumor dataset into either high or low hallmark MYC-V1 pathway score cohorts and performed Virtual Inference of Protein-Activity Enrichment Regulon (VIPER)(Alvarez, Shen et al. 2016, Lachmann, Giorgi et al. 2016) analysis. Comparing

6

138   common replication stress response and DNA damage repair regulons from the VIPER

139   analysis revealed a robust enrichment in tumors with high MYC-V1 pathway scores

140   compared to those with lower MYC-V1 pathway scores (Figure 1C). In PDAC, patient

141   survival and efficacy of treatment is impacted, in part, by somatic alterations in DNA

142   damage response (DDR) genes(Dreyer, Upstill-Goddard et al. 2021, Link, Eng et al.

143   2025). To investigate whether DDR alteration status affects MYC's impact on patient

144   survival, we separated our cohort into four categories that stratify based on high/low

145   Hallmark MYC V1 target score and whether a patient has a detected somatic DDR

146   alteration in their tumor. Patients with MYC-high tumors had poor survival regardless of

147   tumor DDR status (Figure 1D, red vs blue lines); however, patients with DDR-altered

148   MYC-low tumors have a significantly better survival probability over MYC-high DDR-

149   altered tumors (Figure 1D). This suggests that high MYC activity promotes tolerance to

150   the presence of DDR alterations, supporting aggressive tumors and poor patient

151   outcome including resistance to DNA damaging chemotherapy, as 24% of our patients

152   in our cohort received neoadjuvant and/or adjuvant chemotherapy(Link, Eng et al.

153   2025).

154   To investigate these findings at the protein level within human PDAC, we

155   performed cyclic immunofluorescence (cycIF) on a patient-derived PDAC tissue

156   microarray (TMA) with antibodies detecting markers of post-translationally active MYC

157   (phospho-Ser62), cell proliferation, and DNA damage response. Consistently, we

158   observed cytokeratin-19 positive tumor cells with overlapping staining for the activated

159   pS62-MYC(Sears 2004, Hann 2006) and DNA damage markers RAD51, pRPA, and

160   γH2AX (Figure 1E,F). When per cell intensities were quantified and ranked by

7

161 correlation with pS62-MYC in tumor cells, in addition to the DNA damage proteins

162 RAD51, pRPA, γH2AX and 53BP1, we observed significant correlation with cell cycle

163 proteins PCNA and Ki67, suggestive of coupled proliferate and DNA repair (Figure

164 1G,H). However, when quantifying all 54 cores across 34 patients, the correlation

165 between pS62-MYC and proliferation markers is not as strong while the correlation with

166 DNA damage markers remain robust and significant (Figure 1I). Together, this data

167 indicates that MYC expression correlates with markers for DNA damage response in

168 PDAC tumors and impacts overall patient survival, particularly with patients with somatic

169 DDR alterations.

170

171 **MYC is Detected in Proximity to DNA Double-Strand Breaks**

172   To explore whether MYC plays a direct role in the molecular regulation of DNA

173 breaks, we performed DNA Damage in situ Proximity Ligation Assay (DI-PLA) (Galbiati

174 and d'Adda di Fagagna 2019), wherein a biotinylated DNA probe was ligated to DSBs,

175 and proximity ligation assay (PLA) was conducted between biotin and MYC (Figure 2A).

176 We treated an early passage patient-derived cancer cell line (ST-00024058), isolated

177 from a resected PDAC tumor, with bleomycin and conducted DI-PLA. Bleomycin

178 treatment resulted in a significant increase in DI-PLA puncta compared to DMSO

179 control, indicating an enhanced proximity between MYC & DSBs in a patient-derived

180 cancer cell line following DNA-damaging chemotherapy (Figure 2B). In a more precisely

181 controlled system, we leveraged site-specific cleavage with a cas9 transfection with

182 RNA guides targeting the 28S ribosomal DNA (rDNA) (van Sluis and McStay 2015).

183 Targeting rDNA allows for signal amplification since there are approximately 400 copies

8

184 of rDNA per cell. DI-PLA revealed a robust increase in association between MYC and

185 cas9-induce DSBs compared to non-targeting control (NT) (Figure 2C). This suggests

186 that MYC associates with DSBs generated by both chemotherapy and site-specific

187 cleavage.

188 As replication stress is a driver of DSBs and MYC expression correlates with

189 pRPA expression, a marker of stalled replication forks (Figure 1D-G), we sought to

190 determine whether MYC localization to DSBs is increased under high levels of

191 replication stress in cells. To induce replication stress, cells were treated with aphidicolin

192 (APH), an inhibitor of DNA polymerases α, δ, and ε, leading to the formation of

193 vulnerable regions of single-stranded DNA, replication fork collapse, and the

194 subsequent generation of DSBs(Vesela, Chroma et al. 2017). Consistent with direct

195 DSB generation, APH treatment for 5-hours in HEK293, U2OS, MIA PaCa-2, and HeLa

196 cells revealed a significant and robust increase in MYC's association with replication

197 stress-induced DSBs (Figure 2D). In agreement, the MYC-γH2AX PLA signal also

198 increased following APH treatment in these cell lines, together highlighting the presence

199 of MYC at DSBs following replication stress across multiple conventional cell lines

200 (Figure 2E). To begin to understand the influence of MYC's localization to DSBs on DNA

201 repair, we tested whether APH induced an enrichment between MYC and known DNA

202 repair proteins. BRCA1 binds DSBs and promotes homologous recombination directed

203 repair and has been shown to bind to MYC, however, the mechanistic impact of this

204 interaction remains to be clarified (Wang, Zhang et al. 1998, Li, Lee et al. 2002, Epasto,

205 Pötzl et al. 2024). We observed a robust association between MYC and BRCA1

206 following 5-hour APH treatment, suggesting that this interaction is responsive to

207   increased genomic damage (Figure 2F). Furthermore, we detected an APH-induced

208   increase in association between the post-transcriptionally stable form of MYC (pS62-

209   MYC) and RAD51 (Figure 2G); an interaction not previously reported in the literature.

210   Taken together, our data suggests that MYC has a conserved capability of associating

211   with DSBs and is able to interact with DNA repair proteins in response to DNA damage.

212

213   **MYC's Interactome is Enriched for DNA Repair Proteins Under Replication Stress**

214   To survey a broader and more unbiased enrichment of MYC's interactions under

215   replication stress, we generated stably expressed, doxycycline-inducible MYC-BioID2 in

216   HEK293 cells for proximity-dependent labeling (Figure 3A). We treated these cells with

217   either DMSO or APH and detected a total of 1,648 targets (Figure 3B). Our aim was to

218   detect shifts in MYC's interactome following 24-hour APH treatment. However, there

219   were no statistically significant interactors enriched in APH treatment versus DMSO

220   treatment following false discovery rate (FDR) correction (Figure 3C). This limited

221   differential is likely attributed to a technical limitation of the BioID2 system, which

222   requires an 18-hour incubation for biotinylation of proteins, whereas DNA damage

223   response occurs on a much shorter timescale. Nevertheless, after background

224   subtraction of the BioID2-only control and applying a ³2-fold differential abundance

225   threshold and p=0.25 a shift in MYC protein target interactions in response to APH

226   treatment is observed (Figure 3D). To better understand the functional differences of

227   MYC interactors between DMSO and APH conditions, we conducted Gene Ontology

228   (GO) enrichment using the BinGO tool in Cytoscape (Shannon, Markiel et al. 2003,

229   Maere, Heymans et al. 2005, Doncheva, Morris et al. 2019). The interconnections of the

230   enriched gene ontologies for MYC interactors under DMSO emphasize mechanisms

231   which align with MYC's canonical functions involved in gene expression, chromatin

232   remodeling, and metabolism (Figure 3E). The APH-enriched MYC interactor ontologies

233   highlight proteins involved in response to genomic damage, cell cycle regulation, and

234   DNA repair (Figure 3F). These findings are consistent with recent studies demonstrating

235   that under stress conditions, MYC shifts away from driving transcriptional processes to

236   promoting DNA stability(Papadopoulos, Solvie et al. 2022, Solvie, Baluapuri et al. 2022).

237   In agreement, when GO terms are ranked by adjusted p-value, we see the most

238   significant terms for DMSO include processes involved in nucleotide metabolism and

239   gene regulation while top terms for APH-induced MYC interactions pertain to genomic

240   maintenance (Figure 3G). This data indicates that MYC's interactome becomes more

241   enriched for DNA damage response proteins under replication stress.

242

243   **Serine 62 Phosphorylation of MYC Promotes its Association with DSBs**

244   To begin to investigate whether post-translational modification of MYC could play

245   a role in the functional switch in MYC activity upon genomic insult and its localization to

246   DSBs and interaction with repair proteins, we investigated the impact of MYC's

247   phosphorylation status on this mechanism. Phosphorylation of MYC, particularly at

248   threonine 58 and serine 62, have been shown to regulate its stability, target gene

249   promoter binding, and spatial localization within the nucleus(Su, Pelz et al. 2018, Cohn,

250   Liefwalker et al. 2020). In response to growth signals, MYC is transiently stabilized by

251   the phosphorylation of serine 62, enhancing its engagement with target genes, including

252   those poised at the nuclear periphery(Yeh, Cunningham et al. 2004, Vervoorts, Lüscher-

11

253   Firzlaff et al. 2006, Farrell, Pelz et al. 2013, Su, Pelz et al. 2018). Processive

254   phosphorylation at threonine 58 (pT58-MYC) destabilizes MYC, initiating its degradation

255   via the proteosome(Gregory and Hann 2000, Welcker, Orian et al. 2004). To examine

256   whether these phosphorylation sites in MYC could also affect its association with DSBs,

257   we used doxycycline-inducible HEK293 cells which express hemagglutinin (HA) tagged

258   wild-type MYC (WT-MYC), serine-to-alanine mutant MYC (S62A-MYC), or the

259   threonine-to-alanine mutant MYC (T58A-MYC). Given the sequential nature of

260   phosphorylation at these sites, with S62 phosphorylation preceding the phosphorylation

261   of T58 by the processive GSK3 kinase (Gregory, Qi et al. 2003), S62A-MYC lacks

262   phosphorylation at both sites, whereas T58A-MYC exhibits robust phosphorylation at

263   S62 but lacks phosphorylation at T58 (Figure 4A). We performed HA-tagged DI-PLA

264   following cas9-directed cleavage of the 28S rDNA. Consistent with endogenous MYC,

265   we observed a robust increase in the association of ectopic WT-MYC and cas9-induced

266   DSBs (Figure 4B). In contrast, S62A-MYC showed no statistically significant difference

267   between non-targeting (NT) control and cas9-induced DSBs, while T58A-MYC exhibited

268   a similar or even greater induction of MYC associated with DSBs compared to WT.

269   Similar induction patterns were observed in a PLA between HA-tag and γH2AX (Figure

270   4C), demonstrating that serine 62 phosphorylation is a key determinant of MYC's

271   association with cas9-induced DSBs. To confirm these findings under replication-stress

272   induced DSBs, we treated the MYC mutant cells with APH. WT-MYC showed a strong

273   increased association with APH-induced DSBs compared to the DMSO control (Figure

274   4D). Likewise, T58A-MYC demonstrated a robust increase in association with APH-

275   induced DSBs. While the S62A-MYC mutant also showed some increased association

12

276 with DSBs, this was significantly less than WT-MYC and T58A-MYC. T58A-MYC retains

277 persistent serine 62 phosphorylation due to resistance to PP2A-mediated

278 dephosphorylation, unlike WT-MYC (Yeh, Cunningham et al. 2004, Arnold and Sears

279 2006). Notably, T58A-MYC displayed elevated association with DSBs even prior to APH

280 treatment. Collectively, these data indicate that serine 62 phosphorylation plays an

281 important role in MYC's efficient association with DSBs in response to cas9- and APH

282 treatment-induced DSBs. To verify that the difference in association with DSBs was not

283 due to differences in expression levels, whole cell lysates of the three cell lines showed

284 equal expression of the HA-tag MYCs (Figure 4E). In agreement with past findings of

285 negative autoregulation (Kaur and Cole 2013), the lower molecular weight band of

286 endogenous MYC was nearly undetectable when ectopic MYC is expressed, supporting

287 that endogenous MYC did not compensate for the phosphorylation mutants.

288 Furthermore, a neutral comet assay demonstrated that the levels of DSBs induced by 5-

289 hour APH treatment was not significantly different between cells expressing WT-, S62A-,

290 and T58A-MYC, confirming that the number of DSBs is equivalent across the conditions

291 (Figure 4F,G). Taken together, these data underscore the critical role of serine 62

292 phosphorylation in MYC's efficient association with DSBs.

293

294 **Serine 62 Phosphorylation of MYC Regulates the Efficient Recruitment of BRCA1**

295 **and RAD51 to DSBs**

296   To assess whether MYC could influence the recruitment of repair factors to

297 DSBs, we initially evaluated the impact of MYC phosphorylation status on its

298 association with BRCA1 & RAD51 as shown in Figure 2F & G. Both WT & T58A-MYC

13

299   exhibited strong and comparable association with BRCA1 following APH treatment,

300   while S62A-MYC showed a weaker induction, significantly reduced compared to WT &

301   T58A-MYC (Figure 5A). Similarly, WT-MYC demonstrated a pronounced APH-induced

302   increase in RAD51 association, T58A-MYC association was also significantly increased,

303   while S62A-MYC did not show a significantly increased interaction with RAD51 (Figure

304   5B). Co-immunoprecipitation of flag-tagged WT-, S62A-, or T58A-MYC in APH-treated

305   HEK293 cells confirmed the reduced interaction between MYC and RAD51 when serine

306   62 phosphorylation is blocked (Figure 5C). Given S62A-MYC's diminished association

307   with DSBs, we next examined whether serine 62 phosphorylation of MYC and its

308   efficient recruitment to DSBs might be important for the localization of BRCA1 and

309   RAD51 to DSBs. DI-PLA analysis of BRCA1 in WT-MYC expressing cells demonstrated

310   a robust APH-induced increase in BRCA1 association with DSBs (Figure 5D,E).

311   However, this induction was not observed in S62A-MYC expressing cells, with no

312   significant difference in BRCA1 association with DSBs between DMSO and APH

313   treatment in these cells. A similar pattern was observed with cas9-induced DSBs (Figure

314   5F), with the unexpected finding that BRCA1's association with DSBs falls below NT

315   control in S62A-MYC expressing cells, an observation that warrants further

316   experimentation to draw a definitive conclusion. S62A-MYC expressing cells also had a

317   marked reduction in RAD51 localization to APH-induced DSBs compared to WT-MYC

318   expressing cells (Figure 5G,H). These results collectively demonstrate that efficient

319   recruitment of BRCA1 and RAD51 to DSBs as well as their association with MYC is

320   reliant on serine 62 phosphorylation of MYC.

321

14

Phosphorylation of MYC at Serine 62 is Critical for DNA Damage Repair and Cell Survival in Response to APH-induced Stress.

To investigate the biological implications of MYC's association with DSBs and DNA repair machinery, we performed a 3-hour washout experiment following APH treatment. Consistent with Figures 4F & G showing equivalent levels of DNA damage in WT- and S62A-MYC expressing cells, APH treatment produced comparable γH2AX puncta in both WT- and S62A-MYC expressing cells (Figure 6A,B). However, while WT-MYC efficiently resolved many of those γH2AX puncta during the 3-hour washout, the number of puncta increased in S62A-MYC expressing cells. Since γH2AX is not an exclusive marker of DSBs, we performed a neutral comet assay of pre- and post-washout. In agreement, WT-MYC successfully resolved APH-induced DSBs, while S62A-MYC comet tails showed longer comet tails post-washout compared to the pre-washout (Figure 6C,D). To assess whether the deficiency in DNA damage repair observed in S62A-MYC expressing cells impacted cell survival, we conducted a 10-day colony formation assay following a 5-hour APH treatment at varying concentrations. T58A-MYC exhibited a similar number of colonies to WT-MYC, whereas S62A-MYC showed a significant reduction and an impaired ability to recover from APH-induced DNA damage (Figure 6E,F). Altogether, these findings suggest that MYC serine 62 phosphorylation impacts its association with DSBs, the recruitment of DNA repair machinery, and the promotion of DNA repair and cell survival.

15

Discussion

342

343   In this study, we explored the non-canonical role of MYC in DDR and its

344   association with DSBs to elucidate new mechanisms through which MYC drives

345   oncogenesis and cancer cell survival. Our findings underscore a role for MYC in

346   maintaining genomic integrity through mechanisms involving a direct role in DNA repair,

347   and we reveal that MYC's phosphorylation at serine 62 is critical for its proximity to

348   DSBs, recruitment of repair proteins like BRCA1 and RAD51, and overall effectiveness

349   of DNA repair (Figure 5G).

350   Transcriptionally, MYC has been shown to promote genomic maintenance by

351   regulating transcription of several DNA repair proteins including RAD50, RAD51,

352   XRCC2, BRCA1, BRCA2, DNA-PKcs, HUS1, and Ku70 (Luoto, Meng et al. 2010).

353   Furthermore, during S-phase, MYC upregulates expression of homologous

354   recombination-directed repair proteins, RAD51 and HUS1 (Robson, Ward et al. 2011).

355   In our large expression dataset from 289 human PDAC tumors, we demonstrated a

356   positive correlation between MYC target pathway activity and both replication stress and

357   DNA repair pathway activity (Figure 1A & B). Furthermore, high versus low MYC target

358   pathway activity showed increased VIPER activity score for DNA repair proteins and an

359   increase in overall survival for patients who harbor somatic DDR mutations when MYC

360   activity is low, consistent with prior findings that heightened MYC and DDR pathways

361   drive a subset of aggressive PDAC tumors(Link, Eng et al. 2025). This connection may

362   not be exclusive to PDAC given that prior clinical findings have shown that MYC

363   amplification and increased genomic instability drive breast cancer progression and

364   aggressiveness in BRCA1-mutated tumors (Grushko, Dignam et al. 2004). The positive

16

365   correlation between MYC-target pathway activity and replication stress signature,

366   supports the idea that MYC upregulates factors to mitigate the MYC-driven stress

367   induced by accelerated cell cycle progression (Felsher and Bishop 1999). In agreement,

368   MYC, along with MYCN, compensates for heightened replication stress by increasing

369   transcription of components that address stalled replication forks and facilitate DNA

370   repair, including the MRN complexes (Chiang, Teng et al. 2003, Petroni, Sardina et al.

371   2016), Cohesin components (Rohban, Cerutti et al. 2017), TRIM33 (Rousseau, Einig et

372   al. 2023), and MCM10 (Murayama, Takeuchi et al. 2021). In addition, MYC expression

373   induces nucleotide biosynthesis genes to sustain nucleotide balance to reduce

374   replication stress (Liu, Li et al. 2008).

375   Beyond MYC's transcriptional role in genomic maintenance, emerging evidence

376   suggests that MYC protein can directly influences DNA damage prevention and repair.

377   In a study by Cui et al., pS62-MYC colocalized with gH2AX and DNA-PKcs/S2056 foci

378   in irradiated HeLa cells and that MYC silencing reduced DNA repair (Cui, Fan et al.

379   2015). In neuroblastoma, MYCN is found at sites of heightened transcription which have

380   a greater propensity to accumulate DNA damage. At these genomically stressed sites,

381   the ubiquitin-specific protease USP11 was shown to preferentially bind to and stabilize

382   de-phosphorylated threonine 58 MYCN which mediated the recruitment of BRCA1 to

383   stalled RNAPII complexes, preventing the accumulation of deleterious R-loops (Herold,

384   Kalb et al. 2019). In agreement, we showed that MYC's association with DSBs and

385   BRCA1 was greatest in T58A-MYC and diminished in S62A-MYC when compared to

386   WT-MYC (Figures 4,5). Emphasizing that serine 62 phosphorylation is important for

387   MYC's association with DSBs and repair factors.

17

388   MYC elicits its cellular activity through its interactome and by recruiting and

389   concentrating multiprotein complexes at genomic sites across the genome(Lourenco,

390   Resetca et al. 2021, Das, Lewis et al. 2023). Our MYC-BioID2 proteomic screen

391   detected a functional shift in MYC's interactome under replication stress (Figure 3).

392   Under DMSO conditions, MYC-BioID2 biotinylated more interactions with proteins

393   involved in canonical MYC functions that drive gene expression and metabolism while

394   APH-enriched MYC interacting proteins aligned more with DDR pathways. MYC's

395   interactome under cellular stress aligns with observations that MYC forms stress-

396   induced higher-order multimeric structures around stalled replication forks, shielding

397   them from RNAPII (Solvie, Baluapuri et al. 2022). These MYC multimers were also

398   reported to encompass repair proteins such as FANCD2, ATR, and BRCA1, to mitigate

399   transcription-replication conflicts and subsequent DSBs during S-phase. In addition, it

400   was recently shown that MYCN exists in two distinct physical states depending on the

401   phase of the cell cycle. During G1, MYCN heterodimerizes with MAX to drive

402   transcription, whereas during S-phase, MYCN interacts with nuclear exosome targeting

403   complexes responsible for preventing transcription-replication collisions and eliminating

404   genotoxic RNA-structures (Papadopoulos, Solvie et al. 2022, Papadopoulos, Ha et al.

405   2024). These functionally distinct physical states of MYC align with numerous

406   observations that post-translational modifications (PTMs) and protein-protein

407   interactions partition MYC into functionally distinct "MYC-pools" which impacts its

408   stability (Tworkowski, Salghetti et al. 2002, Guo, Li et al. 2014, Lourenco, Resetca et al.

409   2021). Since pS62-MYC, but not pT58-MYC, was shown to be essential for the spatial

410   partitioning of MYC within the nucleus (Su, Pelz et al. 2018), it is plausible that

411 phosphorylation at threonine 58 and serine 62 regulates functionally distinct MYC-pools

412 under different cellular contexts. For example, MYC assembles and recruits a

413 topiosome composed of topoisomerases 1 and 2 to alleviate transcription-induced

414 topological stress (Das, Kuzin et al. 2022). However, in the presence of excessive DNA

415 damage in cell lines, MYC is degraded and replaced with a p53-mediated topiosome,

416 leading to proficient DDR and repair (Das, Karmakar et al. 2024). MYC also requires

417 ubiquitination and degradation for the transfer of PAF1c to RNAPII to couple

418 transcriptional elongation with DSB repair (Endres, Solvie et al. 2021). The notion that

419 MYC-pools are independently regulated spatially, could help explain reports that MYC is

420 degraded in response to DNA damage (Popov, Wanzel et al. 2007, Britton, Salles et al.

421 2008, Li, Challagundla et al. 2015), since a subset of more stable MYC pools, such as

422 pS62-MYC, could allow for prolonged repair. Furthermore, since pS62-MYC is required

423 for the efficient recruitment of BRCA1 and RAD51 to DSBs, MYC may play a role in

424 directing homologous-directed repair. Future studies will investigate the consequences

425 of MYC-directed repair in PDAC.

426 In conclusion, this study provides novel mechanistic understanding into the non-

427 canonical role of MYC in DSB repair, demonstrating that serine 62 phosphorylation is

428 critical for directing MYC's efficient association with DSBs and subsequent recruitment

429 of repair factors necessary for productive DNA repair and cell survival under stress.

430 These insights advance our understanding of MYC's function beyond transactional

431 regulation, highlighting additional contributions to MYC-driven oncogenesis and

432 resistance to DNA damaging chemotherapy.

433 **Methods**

434 **Cell Lines**

435 MIA PaCa2, U2OS, HeLa, HEK293 and MYC-mutant HA-tag HEK293TR cells were

436 maintained in DMEM supplemented with 10% characterized fetal bovine serum (FBS),

437 2mM L-glutamine, and 1X penicillin/streptomycin at 37°C and 5% CO_2. Patient derived

438 cell line ST-00024058 was generated as previously described (Queitsch, Moore et al.

439 2023).

440 **Generation of stable inducible 293TR-MYC cells**

441 293TR-MYC inducible cells were generated using a technique as previously described

442 (Farrell, Pelz et al. 2013). Briefly, HEK293 cells were infected with lentivirus encoding

443 the Tet repressor, pLenti6/TR (Invitrogen) for 12 hours. Stable clones were maintained

444 at 5μg/mL blasticidin (Invitrogen). Clones were then infected with lentivirus expressing

445 HA-MYC (pLenti4/TO/CMV-HA-MYC). Cells were selected with 200 μg/mL Zeocin

446 (Invitrogen) for 10 days until clones grew out. Clones were screened for HA-MYC when

447 treated with 1μg/mL doxycycline for 24 hours. Stable 293TR-MYC^{T58A} and 293TR-

448 MYC^{S62A} cells were similarly constructed except with pLenti4/TO/CMV-HA-MYC^{T58A} or

449 pLenti4/TO/CMV-HA-MYC^{S62A} respectively.

450 **Tissue acquisition and patient consent**

451 Patient blood, tissues, and data were acquired with inform consent aligned with the

452 Declaration of Helsinki and were obtained through the Oregon Pancreas Tissue

453 Registry under Oregon Health & Science University IRB protocol #3609.

454 **RNA-sequencing of patient PDAC**

20

455   Detailed methods for RNA preparation and sequencing can be found in Link et al (Link,

456   Pelz et al. 2022). OHSU supplied formalin-fixed paraffin-embedded tissue sections to

457   Tempus as part of a contract agreement. Tempus performed whole-transcriptome RNA

458   sequencing as previously described (Beaubier, Tell et al. 2019).

459   **Gene Set Variation Analysis (GSVA)**

460   GSVA analysis(Hänzelmann, Castelo et al. 2013) along with the MSigDB database

461   v7.5.1 Hallmark gene set collection (Liberzon, Birger et al. 2015) was used to calculate

462   Hallmark scores for all primary tumors. The replication stress gene set was derived from

463   replication stress-induced gene expression patterns observed in Dreyer et al (Dreyer,

464   Upstill-Goddard et al. 2021). We compiled this composite gene set from all genes the

465   appeared in 3 or more of the 21 gene sets identified by Dreyer et al as being activated

466   in replication stress and DNA damage response. Pearson's correlation coefficient and p-

467   values were calculated using the cor.test() function in R.

468   **VIPER analysis of high vs low Hallmark MYC-V1 score**

469   Transcriptional regulon enrichment was analyzed using VIPER alongside the ARACNe-

470   inferred TCGA PAAD network(Alvarez, Shen et al. 2016, Lachmann, Giorgi et al. 2016).

471   Before running VIPER, gene expression data were normalized by median centering and

472   scaling, and the resulting regulon scores from all primary samples were used for cohort

473   comparisons. For the Gene Ontology (GO)(Ashburner, Ball et al. 2000, Aleksander,

474   Balhoff et al. 2023) enrichment analysis of regulons elevated for the high Hallmark

475   MYC-V1 target pathway cohort, we utilized the R package ClusterProfiler (v.4.6.2)(Wu,

476   Hu et al. 2021). Primary tumors were ranked based on the

477   HALLMARK_MYC_TARGETS_V1 GSVA score to produce quartiles. We then

21

478   compared the top quartile to the bottom quartile and calculated multiple test corrected p-

479   values (q-values) and difference in means between these quartiles for all Viper features.

480   The enrichGO function was configured to assess GO biological process terms, with both

481   p-value and q-value thresholds set to 0.05, and all regulons used as the background.

482   Jaccard similarity was computed using the default setting of the pairwise_termsim.

483   **Cyclic Immunofluorescence multiplex imaging analysis**

484   A PDAC tissue microarray (TMA) was created at OHSU using FFPE blocks from tumors

485   with 1-2 cores per tumor from 34 primary tumors, totaling 55 cores.

486   Immunofluorescence preparation and analysis conducted as previously described(Eng,

487   Bucher et al. 2022). Briefly, images were scanned with Zeiss Axioscan Z1, acquired,

488   stitched, and exported as TIFF format with Zeiss Zen Blue software (v.2.3). Image

489   registration was performed using MATLAB (v.9.11.0), and cellular segmentation was

490   carried out using either Cellpose(Stringer, Wang et al. 2021) or Mesmer(Greenwald,

491   Miller et al. 2022). Unsupervised clustering of individual cell mean fluorescence intensity

492   was used to classify cell types, using the Leiden algorithm implemented in scanpy

493   (v.1.9.3)(Wolf, Angerer et al. 2018). Pearson correlation r of tumoral single-cell mean

494   intensity of DNA damage and proliferation markers with pMYC was calculated in each

495   core. For hypothesis testing, Pearson's r values were transformed with Fisher's Z and

496   95% confidence intervals calculated.

497   **DNA Damage In Situ Ligation followed Proximity Ligation Assay (DI-PLA)**

498   This protocol is adapted from Galbiati et al (Galbiati and d'Adda di Fagagna 2019). Cells

499   are grown on 13mm coverslips and fixed in 4% PFA for 10 minutes at room temperature

500   followed by two washes with PBS.

22

501 *DI-PLA: Blunting*

502 Coverslips are washed twice for 5 minutes with NEB2 buffer (50mM NaCl, 10mM Tris-

503 HCl pH 8, 10mM $MgCl_2$, 1mM DTT, 0.1% Triton X-100) and twice for 5 minutes with

504 Blunting buffer (50mM NaCl, 10mM Tris-HCl pH 7.5, 10mM $MgCl_2$, 5mM DTT, 0.025%

505 Triton X-100). Coverslips are then inverted onto a 35μL drop on parafilm of NEB

506 Blunting Reaction (NEB, E1201): (1mM dNTPs, 1X Blunting Buffer, 0.2mg/mL BSA, 1X

507 Blunting Enzyme). Coverslips are incubated in a dark humidity chamber for 1hr at room

508 temperature.

509 *DI-PLA: Ligation*

510 Coverslips are washed twice for 5 minutes with NEB2 buffer (50mM NaCl, 10mM Tris-

511 HCl pH 8, 10mM $MgCl_2$, 1mM DTT, 0.1% Triton X-100) the twice for 5 minutes with

512 ligation buffer (50mM Tris-HCl pH 7.5, 10mM $MgCl_2$, 10mM DTT, 1mM ATP). Coverslips

513 are then inverted onto a 50μL drop on parafilm of Ligation Reaction (0.1μM DI-PLA

514 Linker, 1X T4 Ligation Buffer (NEB, B0202), 1mM ATP, 0.2 mg/mL BSA, 1X T4 Ligase

515 (NEB, M0202)) overnight at 4$°$C in dark humidity chamber followed by proximity ligation

516 assay between biotin and protein of interest.

517 *DI-PLA Linker*:

518 5'-TACTACCTCGAGAGTTACGCTAGGGATAACAGGGTAATATAGTTT [BtndT]

519 TTTCTATATTACCCTGTTATCCCTAGCGTAACTCTCGAGGTAGTA -3'

520 **Proximity Ligation Assay**

521 Proximity Ligation Assay was performed without deviation from manufacturer's

522 instructions (DUO92008). Single-antibody controls were performed to ensure specificity

523 of antibodies. Coverslips were washed in a 0.5mL volume and reactions were

524 performed by inverting the coverslip onto a 35μL drop on parafilm. Following the

525 proximity ligation reaction, cells stained with DAPI (0.2ug/mL) for 3 minutes followed by

526 one wash in PBS and one water wash. The cells were then inverted and mounted on

527 glass coverslips with 15μL of prolong gold mounting media (LifeTech, P36934) & were

528 cured overnight in the dark at room temperature. A minimum of 30 cells were imaged

529 per replicate at 63X on a Zeiss LSM880 confocal microscope and analyzed with

530 CellProfiler. Statistical significance was performed using two-tailed student's t-test or

531 one-way ANOVA with multiple comparisons. Antibodies used are as follows: MYC

532 (Abcam, 32072), pS62-MYC (Abcam, 78318), Biotin (Sigma, B7653), Biotin (Abcam,

533 53494), RAD51 (Abcam, 133534), HA-tag (ABM, G036), pRPA2 (Novus, NB100-544),

534 γH2AX (Invitrogen, MA12022), γH2AX (Cell Signaling, 9718S), BRCA1 (Santa Cruz,

535 6954), BRCA1 (Sigma, 07-434-MI).

536 **Cas9-Transfection**

537 Cells were cultured on glass coverslips and transiently transfected using Lipofectamine

538 CRISPRMAX (Thermo, #CMAX00015) with TrueCut Cas9 Protein v2 (Thermo,

539 #A36499) and synthetic guide RNA from Invitrogen TrueGuide Synthetic sgRNA (Cat#:

540 35514) or Negative Control (Cat#: A35526) following manufacturer's instructions. After

541 8-hour incubation, cells were fixed in 4% paraformaldehyde for 10 minutes at room

542 temperature, washed three times with PBS, and stored at 4°C. The following two rDNA

543 guides were used in a 1:1 ratio of rDNA guide 1: CGAGAGAACAGCAGGCCCGC and

544 rDNA guide 3: GATTTCCAGGGACGGCGCCT.

545 **Western Blot**

24

546   MYC-Mutant expressing HEK293 cells were seeded into 6-well chamber well. The next

547   day, cells were treated with 0.5μg/mL doxycycline for 18 hours then treated with 5μM

548   aphidicolin for 5 hours. Cells were then washed three times with DPBS and flash frozen

549   at -70°C. Cells were then thawed and scraped in lysis buffer (20mM Tris-HCl pH7.5,

550   50mM NaCl, 0.5% Triton X-100, 0.5% DOC, 0.5% SDS, 1mM EDTA, protease inhibitor

551   (Millipore Sigma: 5892791001), and phosphatase inhibitor (Millipore Sigma:

552   4906837001). Lysates were then sonicated with a Branson Sonifier 450 for 10 pulses,

553   Duty factor of 20, and an output of 2. Protein content was then quantified and 25μg of

554   protein was boiled in 1X SDS buffer (50mM Tris-Cl pH 6.8, 2%SDS, 6% glycerol, 5% 2-

555   mercaptoethanol). Samples were loaded into a 4-12% Bis-Tris Citerion Gel (BioRad:

556   345-0123) and run for 1.5 hours at 180V on ice in XT-MOPS (BioRad: 161-0788). The

557   gel is then transferred onto an Immobilin PVDF membrane (Fisher Scientific:

558   IPFL00010) for 90 minutes at 400mA. Membrane is then blocked for 1 hour at room

559   temperature in Aquablock (Arlington Scientific: NC2580736) then incubated overnight

560   with primary antibody. The following day, the membrane is washed for three times with

561   TBST and incubated with secondary Licor antibody for 1 hour in the dark room

562   temperature and imaged on a Licor Odyssey scanner. Antibodies used are as follows:

563   MYC (Abcam, 32072), HA-tag (ABM, G036), pRPA2 (Novus, NB100-544), γH2AX

564   (Invitrogen, MA12022), GAPDH (Fisher, AM4300). Anti-rabbit IgG 800CW (VMR,

565   102673-330), Anti-mouse IgG 680RD (LI-COR, 926-68072), Anti-mouse IgG 800CW

566   (Fisher, NC9401841).

567   **BioID2 Cloning**

568   BioID2 sequence with a five-glycine linker (Addgene: 74224) was cloned at the N-

569   terminus of C-MYC (Addgene: 16011) and inserted into pcDNA4/TO (Invitrogen:

570   V102020) via HindIII (NEB: R0104T) and NotI (NEB: R0189L). The HA-BioID2 only

571   control sequence (Invitrogen: 74224) was cloned into pcDNA4/TO via HindIII and BspEI

572   (NEB: R0540) Each plasmid was independently transfected using Lipofectamine 3000

573   (Thermo Fisher Scientific L3000-015) into HEK293 cells which contained pcDNA6/TR

574   (Invitrogen: V102520) under blasticidin selection at 20ug/mL. Single cell clones were

575   isolated after several days of Zeocin selection at 200ug/mL. MYC-BioID2 positive

576   clones were identified by western blot for biotin and MYC expression upon doxycycline

577   induction (1ug/mL for 24 hours) with Strepavidin 680 (LI-COR Biosciences 926-68079)

578   and Y69 (Abcam ab32072). HA-BioID2 positive clones were screened using a HA-tag

579   antibody (Applied Biological Materials G036).

580   **MYC-BioID2 Assay**

581   Cells were plated on two 15-cm dishes per condition to achieve 80% confluency upon

582   treatment. Cells were treated for 24-hours with 1 µg/mL doxycycline in combination with

583   either 5 µM APH or DMSO vehicle control. For biotinylation, cells were treated with 50

584   µM biotin (Millipore Sigma: B4501) for 18 hours. After treatment, cells were washed

585   twice with PBS and frozen at -70°C and stored until three biological replicates were

586   obtained. Cells were then lysed with 1.5 mL/dish of lysis buffer (50 mM Tris-Cl, pH 7.4,

587   150 mM NaCl, 1% Triton X-100, 0.1% SDS; 1 mM DTT, protease inhibitor (Millipore

588   Sigma: 5892791001), and phosphatase inhibitor (Millipore Sigma: 4906837001), and

589   incubated on ice for 10 minutes. Lysates were scraped, pooled, and sonicated with a

590   Branson Sonifier 450 for two 30-pulse sessions at a 30% duty cycle and 1.5 output, with

591   a 2-minute ice interval. Samples were diluted with 2.6 mL pre-chilled 50 mM Tris-Cl (pH

592   7.4) and sonicated for an additional 30 pulses. Lysates were centrifuged at 16,500 x g

593   for 10 minutes at 4°C to remove debris. 150 µL/condition of Streptavidin-agarose beads

594   (Millipore Sigma: 69203-3) were equilibrated in a 1:1 mixture of lysis buffer and 50 mM

595   Tris-Cl (pH 7.4) and briefly spun down at 8,000 rpm for 2 minutes. Supernatants were

596   transferred to the beads and incubated overnight on a rotator at 4°C. After incubation,

597   beads were washed twice with wash buffer 1 (50 mM HEPES pH 7.5, 400 mM NaCl, 1%

598   Triton X-100, 0.1% deoxycholic acid, 1 mM EDTA) for eight minutes, twice with wash

599   buffer 2 (10 mM Tris-Cl pH 7.4, 500 mM LiCl, 0.5% NP-40, 0.5% deoxycholic acid, 1

600   mM EDTA) at room temperature. Beads were washed once in 50 mM Tris-Cl (pH 7.4)

601   followed by three washes with 100mM ammonium bicarbonate. Beads were

602   resuspended in 100 µL of 100mM ammonium bicarbonate (pH 8) and underwent

603   trypsinization with the addition of 15µL of 80ng/µL trypsin (1.6ug) in 50mM Triethyl

604   ammonium bicarbonate and incubated for 17 hours at 37°C with shaking. After

605   trypsinization, beads were isolated, supernatant removed and filtered with 0.22µm

606   Millipore filter. Filtered sample was dried and dissolved in 20µL of 5% formic acid and

607   injected into Thermo QExactive HF mass spectrometer and run with the 90min LC/MS

608   method. Survey mass spectra were acquired over m/z 375−1400 at 120,000 resolution

609   (m/z 200) and data-dependent acquisition selected the top 10 most abundant precursor

610   ions for tandem mass spectrometry by HCD fragmentation using an isolation width of

611   1.2 m/z, normalized collision energy of 30, and a resolution of 30,000. Dynamic

612   exclusion was set to auto, charge state for MS/MS +2 to +7, maximum ion time 100ms,

613   minimum AGC target of 3 x 106 in MS1 mode and 5 x 103 in MS2 mode. Mass

27

614   spectrometry data from all samples was processed using COMET/PAWS against

615   Uniprot Human database. Comet (v. 2016.01, rev. 3)(Eng, Jahan et al. 2013) was used

616   to search MS2 Spectra against a January 2024 version of canonical FASTA protein

617   database containing human uniprot sequences, and concatenated sequence-reversed

618   entries to estimate error thresholds. Comet searches for all samples were performed

619   with trypsin enzyme specificity with monoisotopic parent ion mass tolerance set to 1.25

620   Da and monoisotopic fragment ion mass tolerance set at 1.0005 Da and a variable

621   modification of +15.9949 Da on Methionine residues.

622   **Protein interaction ontology analysis**

623   BioID2-only detected spectral counts were subtracted from MYC-BioID2 to remove

624   background biotinylation and spectral counts from MYC-BioID2 samples treated with

625   either DMSO or APH were normalized by scaling the average total spectral counts

626   across samples. Log2 fold changes were computed between APH- and DMSO-treated

627   samples, and statistical significance was assessed using two-sided t-test followed by

628   a Benjamini-Hochberg correction. Ontological analysis of targets which pass the 2-fold

629   differential abundance threshold was determined with the BinGO tool in

630   Cytoscape(Shannon, Markiel et al. 2003, Maere, Heymans et al. 2005, Doncheva,

631   Morris et al. 2019).

632   **Neutral comet assay**

633   Cells were plated in 6-well plate and treated with either DMSO control or 5mM

634   aphidicolin for 5-hours. A positive control of 1-hour 100mg/mL bleomycin was included.

635   Glass slides were pre-coated in 1% normal melting point agarose and dried at room

636   temperature. Cells were trypsinized, counted, and resuspended in PBS to 0.35×10^6

28

637   cells/mL on ice. Cell suspensions were combined with molten 1% low-melting-point

638   agarose at a 1:10 (v/v) ratio, then 200 µL of this mixture was applied to pre-coated

639   slides labeled in pencil. Coverslips were added for even distribution, and slides were

640   solidified at 4 °C for 10 minutes in the dark. Slides were then submerged in 4°C lysis

641   buffer (2.5 M NaCl, 100 mM EDTA, 10 mM Tris, 200 mM NaOH, 1% sarcosinate, and

642   1% Triton X-100, pH 10) for 18-hours. Slides were equilibrated in neutral

643   electrophoresis buffer (100mM Tris and 300mM sodium acetate, pH 9) at 4°C for 30

644   minutes and transferred to an electrophoresis chamber with chilled buffer.

645   Electrophoresis was conducted at 1 V/cm for 30 minutes at 4 °C. Slides were immersed

646   in DNA precipitation solution (1M ammonium acetate in 80% ethanol) for 30 minutes,

647   followed by a 30-minute rinse in 70% ethanol at room temperature. Slides were dried at

648   37 °C, then stained with SYBR Green (1:2000, Thermo cat#: S33102) for 15 minutes in

649   the dark. Following a brief rinse in dH2O, slides were dried partially and stored. Images

650   were acquired at 10x using a BioTek Cytation 5 microscope. Comets analyzed using

651   ImageJ software plugin, OpenComet(Gyori, Venkatachalam et al. 2014). Olive Tail

652   Moment (OTM) was calculated using the following equation.

653
$$OTM = \frac{Tail.mean - Head.mean}{100} \times Tail\%DNA$$

654   **Co-Immunoprecipitation**

655   HEK293 cells were transfected with plasmids using Lipofectamine 2000 (Life

656   Technologies) following the manufacturers' protocols. The cells were harvested at 36–

657   48 h post-transfection, washed with PBS and then lysed in ice-cold lysis buffer

658   consisting of 30 mM Tris-HCl (pH 8.0), 0.5% Nonidet P-40, 1 mM EDTA, 1 mM EGTA,

659   200 mM NaCl, 1 mM phenylmethylsulfonyl fluoride, 1 mM DTT, 1 µg/mL pepstatin A,

660   and 1 mM leupeptin and 1mM β-Glycerophosphate with sonication. Equal amounts of

661   clear cell lysate were incubated with anti-Flag M2 agarose beads for 5 hours at 4°C.

662   The beads were washed 5 times with lysis buffer. Bound proteins were detected by

663   immunoblot using antibodies, as indicated in Figure legends.

664   **Immunofluorescence staining**

665   HEK293 cells with either HA-MYC or S62A-MYC were plated on poly-D-lysine treated

666   glass coverslips and incubated for 24-hours. Expression was induced with 0.5µg/mL

667   doxycycline for 18-hours then treated with 5µM APH or DMSO for 5-hours. Cells were

668   then either fixed with 4% paraformaldehyde for 10 minutes or media change with dox for

669   3-hours followed by fixation. Coverslips were then permeabilized with 0.25% Triton X-

670   100 for 10 minutes followed by a 1-hour block (10% goat serum, 0.1% Triton X-100).

671   Coverslips were then incubated in primary antibody (gH2AX, Cell Signaling, 9718S)

672   overnight at RT. Cells were then washed in three times in 1X PBS for 10 minutes and

673   incubated in secondary antibody (Jackson Immuno, 111-565-144) for 2 hours at RT.

674   Coverslips are washed again for three times in 1X PBS and stained with 0.2µg/mL DAPI

675   for 3 minutes, mounted (LifeTech, P36934), and cured overnight in the dark at room

676   temperature. Coverslips were imaged at 63X on a Zeiss LSM880 confocal microscope

677   and puncta were analyzed with CellProfiler (www.cellprofiler.org) (Stirling, Swain-

678   Bowden et al. 2021).

679   **Colony formation assay**

680   Cells were treated in a 6-well plate then trypsinized, counted, and plated at 1,000

681   cells/well of a 12-well plate. Media was changed every three days with the addition of

682   0.5µg/mL doxycycline. After 10 days, the media was removed and stained with 0.5%

683   crystal violet in 50% ethanol for 30 minutes. The excess dye was then gently washed

684   away with slow-running water. The plates were then dried at RT and colonies were

685   counted.

Competing Interest Statement

RCS reports consulting services to Novartis, RAPPTA Therapeutics, and Larkspur. JRB declares SAB for Perthera, Advisory for IDEAYA and is an editor for Taylor & Francis publishing.

Acknowledgements

Author Contributions

GMC and RCS contributed to the project design; GMC performed and analyzed all experiments unless otherwise stated; CP analyzed RNA-sequencing data; KC stained tumor microarray and JE analyzed tumor microarray; CDL is the principal investigator of the clinical trial which lead to the created of PDAC patient-derived cell lines; JRB developed technology for deriving patient-derived cell lines; AS assisted in the generation and classification of the patient-derived PDAC cell line, ST-00024058; CJD & GMC designed and executed MYC-BioID2 experiments and analysis with bioinformatic

32

709   help from CP; XXS & MD performed Co-Immunoprecipitation experiment. GMC wrote

710   the paper with edits and revisions from RCS and CJD. All authors have approved the

711   current version of the manuscript.

References

Aleksander, S. A., J. Balhoff, S. Carbon, J. M. Cherry, H. J. Drabkin, D. Ebert, M. Feuermann, P. Gaudet, N. L. Harris, D. P. Hill, et al. (2023). "The Gene Ontology knowledgebase in 2023." Genetics **224**(1).

Alvarez, M. J., Y. Shen, F. M. Giorgi, A. Lachmann, B. B. Ding, B. H. Ye and A. Califano (2016). "Functional characterization of somatic mutations in cancer using network-based inference of protein activity." Nat Genet **48**(8): 838-847.

Arnold, H. K. and R. C. Sears (2006). "Protein phosphatase 2A regulatory subunit B56alpha associates with c-myc and negatively regulates c-myc accumulation." Mol Cell Biol **26**(7): 2832-2844.

Ashburner, M., C. A. Ball, J. A. Blake, D. Botstein, H. Butler, J. M. Cherry, A. P. Davis, K. Dolinski, S. S. Dwight, J. T. Eppig, et al. (2000). "Gene ontology: tool for the unification of biology. The Gene Ontology Consortium." Nat Genet **25**(1): 25-29.

Beaubier, N., R. Tell, D. Lau, J. R. Parsons, S. Bush, J. Perera, S. Sorrells, T. Baker, A. Chang, J. Michuda, et al. (2019). "Clinical validation of the tempus xT next-generation targeted oncology sequencing assay." Oncotarget **10**(24): 2384-2396.

Britton, S., B. Salles and P. Calsou (2008). "c-MYC protein is degraded in response to UV irradiation." Cell Cycle **7**(1): 63-70.

Chen, H., H. Liu and G. Qing (2018). "Targeting oncogenic Myc as a strategy for cancer treatment." Signal Transduct Target Ther **3**: 5.

Chiang, Y.-C., S.-C. Teng, Y.-N. Su, F.-J. Hsieh and K.-J. Wu (2003). "c-Myc Directly Regulates the Transcription of the NBS1 Gene Involved in DNA Double-strand Break Repair *." Journal of Biological Chemistry **278**(21): 19286-19291.

Cohn, G. M., D. F. Liefwalker, E. M. Langer and R. C. Sears (2020). "PIN1 Provides Dynamic Control of MYC in Response to Extrinsic Signals." Frontiers in Cell and Developmental Biology **8**.

Cui, F., R. Fan, Q. Chen, Y. He, M. Song, Z. Shang, S. Zhang, W. Zhu, J. Cao, H. Guan, et al. (2015). "The involvement of c-Myc in the DNA double-strand break repair via regulating radiation-induced phosphorylation of ATM and DNA-PKcs activity." Mol Cell Biochem **406**(1-2): 43-51.

Dang, C. V. (2012). "MYC on the path to cancer." Cell **149**(1): 22-35.

Das, S. K., S. Karmakar, H. Venkatachalapathy, R. K. Jha, E. Batchelor and D. Levens (2024). "Excessive MYC-topoisome activity triggers acute DNA damage, MYC degradation, and replacement by a p53-topoisome." Mol Cell **84**(21): 4059-4078.e4010.

Das, S. K., V. Kuzin, D. P. Cameron, S. Sanford, R. K. Jha, Z. Nie, M. T. Rosello, R. Holewinski, T. Andresson, J. Wisniewski, et al. (2022). "MYC assembles and stimulates topoisomerases 1 and 2 in a "topoisome"." Mol Cell **82**(1): 140-158.e112.

Das, S. K., B. A. Lewis and D. Levens (2023). "MYC: a complex problem." Trends Cell Biol **33**(3): 235-246.

Devaiah, B. N., J. Mu, B. Akman, S. Uppal, J. D. Weissman, D. Cheng, L. Baranello, Z. Nie, D. Levens and D. S. Singer (2020). "MYC protein stability is negatively regulated by BRD4." Proceedings of the National Academy of Sciences **117**(24): 13457-13467.

754 Doncheva, N. T., J. H. Morris, J. Gorodkin and L. J. Jensen (2019). "Cytoscape StringApp:
755 Network Analysis and Visualization of Proteomics Data." J Proteome Res **18**(2): 623-632.
756 Dreyer, S. B., R. Upstill-Goddard, V. Paulus-Hock, C. Paris, E. M. Lampraki, E. Dray, B.
757 Serrels, G. Caligiuri, S. Rebus, D. Plenker, et al. (2021). "Targeting DNA Damage Response
758 and Replication Stress in Pancreatic Cancer." Gastroenterology **160**(1): 362-377.e313.
759 Endres, T., D. Solvie, J. B. Heidelberger, V. Andrioletti, A. Baluapuri, C. P. Ade, M. Muhar, U.
760 Eilers, S. M. Vos, P. Cramer, et al. (2021). "Ubiquitylation of MYC couples transcription
761 elongation with double-strand break repair at active promoters." Mol Cell **81**(4): 830-
762 844.e813.
763 Eng, J., E. Bucher, Z. Hu, T. Zheng, S. L. Gibbs, K. Chin and J. W. Gray (2022). "A framework
764 for multiplex imaging optimization and reproducible analysis." Commun Biol **5**(1): 438.
765 Eng, J. K., T. A. Jahan and M. R. Hoopmann (2013). "Comet: an open-source MS/MS
766 sequence database search tool." Proteomics **13**(1): 22-24.
767 Epasto, L. M., C. Pötzl, H. Peterlik, M. Khalil, C. Saint-Pierre, D. Gasparutto, G. Sicoli and D.
768 Kurzbach (2024). "NMR-identification of the interaction between BRCA1 and the
769 intrinsically disordered monomer of the Myc-associated factor X." Protein Sci **33**(1): e4849.
770 Farrell, A. S., C. Pelz, X. Wang, C. J. Daniel, Z. Wang, Y. Su, M. Janghorban, X. Zhang, C.
771 Morgan, S. Impey, et al. (2013). "Pin1 regulates the dynamics of c-Myc DNA binding to
772 facilitate target gene regulation and oncogenesis." Mol Cell Biol **33**(15): 2930-2949.
773 Felsher, D. W. and J. M. Bishop (1999). "Transient excess of MYC activity can elicit genomic
774 instability and tumorigenesis." Proc Natl Acad Sci U S A **96**(7): 3940-3944.
775 Fernandez, P. C., S. R. Frank, L. Wang, M. Schroeder, S. Liu, J. Greene, A. Cocito and B.
776 Amati (2003). "Genomic targets of the human c-Myc protein." Genes Dev **17**(9): 1115-1129.
777 Frank, S. R., T. Parisi, S. Taubert, P. Fernandez, M. Fuchs, H. M. Chan, D. M. Livingston and
778 B. Amati (2003). "MYC recruits the TIP60 histone acetyltransferase complex to chromatin."
779 EMBO Rep **4**(6): 575-580.
780 Gabay, M., Y. Li and D. W. Felsher (2014). "MYC activation is a hallmark of cancer initiation
781 and maintenance." Cold Spring Harb Perspect Med **4**(6).
782 Galbiati, A. and F. d'Adda di Fagagna (2019). "DNA Damage In Situ Ligation Followed by
783 Proximity Ligation Assay (DI-PLA)." Methods Mol Biol **1896**: 11-20.
784 Greenwald, N. F., G. Miller, E. Moen, A. Kong, A. Kagel, T. Dougherty, C. C. Fullaway, B. J.
785 McIntosh, K. X. Leow, M. S. Schwartz, et al. (2022). "Whole-cell segmentation of tissue
786 images with human-level performance using large-scale data annotation and deep
787 learning." Nat Biotechnol **40**(4): 555-565.
788 Gregory, M. A. and S. R. Hann (2000). "c-Myc proteolysis by the ubiquitin-proteasome
789 pathway: stabilization of c-Myc in Burkitt's lymphoma cells." Mol Cell Biol **20**(7): 2423-2435.
790 Gregory, M. A., Y. Qi and S. R. Hann (2003). "Phosphorylation by glycogen synthase kinase-3
791 controls c-myc proteolysis and subnuclear localization." J Biol Chem **278**(51): 51606-
792 51612.
793 Grushko, T. A., J. J. Dignam, S. Das, A. M. Blackwood, C. M. Perou, K. K. Ridderstråle, K. N.
794 Anderson, M.-J. Wei, A. J. Adams, F. G. Hagos, et al. (2004). "MYC Is Amplified in BRCA1-
795 Associated Breast Cancers." Clinical Cancer Research **10**(2): 499-507.

796 Guo, J., T. Li, J. Schipper, K. A. Nilson, F. K. Fordjour, J. J. Cooper, R. Gordân and D. H. Price
797 (2014). "Sequence specificity incompletely defines the genome-wide occupancy of Myc."
798 Genome Biology 15(10): 482.
799 Gyori, B. M., G. Venkatachalam, P. S. Thiagarajan, D. Hsu and M.-V. Clement (2014).
800 "OpenComet: An automated tool for comet assay image analysis." Redox Biology 2: 457-
801 465.
802 Hann, S. R. (2006). "Role of post-translational modifications in regulating c-Myc
803 proteolysis, transcriptional activity and biological function." Semin Cancer Biol 16(4): 288-
804 302.
805 Hann, S. R. and R. N. Eisenman (1984). "Proteins encoded by the human c-myc oncogene:
806 differential expression in neoplastic cells." Mol Cell Biol 4(11): 2486-2497.
807 Hänzelmann, S., R. Castelo and J. Guinney (2013). "GSVA: gene set variation analysis for
808 microarray and RNA-Seq data." BMC Bioinformatics 14(1): 7.
809 Herold, S., J. Kalb, G. Büchel, C. P. Ade, A. Baluapuri, J. Xu, J. Koster, D. Solvie, A.
810 Carstensen, C. Klotz, et al. (2019). "Recruitment of BRCA1 limits MYCN-driven
811 accumulation of stalled RNA polymerase." Nature 567(7749): 545-549.
812 Jha, R. K., F. Kouzine and D. Levens (2023). "MYC function and regulation in physiological
813 perspective." Front Cell Dev Biol 11: 1268275.
814 Kaur, M. and M. D. Cole (2013). "MYC Acts via the PTEN Tumor Suppressor to Elicit
815 Autoregulation and Genome-Wide Gene Repression by Activation of the Ezh2
816 Methyltransferase." Cancer Research 73(2): 695-705.
817 Kim, J., A. J. Woo, J. Chu, J. W. Snow, Y. Fujiwara, C. G. Kim, A. B. Cantor and S. H. Orkin
818 (2010). "A Myc network accounts for similarities between embryonic stem and cancer cell
819 transcription programs." Cell 143(2): 313-324.
820 Kumari, A., W. P. Folk and D. Sakamuro (2017). "The Dual Roles of MYC in Genomic
821 Instability and Cancer Chemoresistance." Genes 8(6): 158.
822 Lachmann, A., F. M. Giorgi, G. Lopez and A. Califano (2016). "ARACNe-AP: gene network
823 reverse engineering through adaptive partitioning inference of mutual information."
824 Bioinformatics 32(14): 2233-2235.
825 Li, H., T. H. Lee and H. Avraham (2002). "A novel tricomplex of BRCA1, Nmi, and c-Myc
826 inhibits c-Myc-induced human telomerase reverse transcriptase gene (hTERT) promoter
827 activity in breast cancer." J Biol Chem 277(23): 20965-20973.
828 Li, Y., K. B. Challagundla, X. X. Sun, Q. Zhang and M. S. Dai (2015). "MicroRNA-130a
829 associates with ribosomal protein L11 to suppress c-Myc expression in response to UV
830 irradiation." Oncotarget 6(2): 1101-1114.
831 Liberzon, A., C. Birger, H. Thorvaldsdóttir, M. Ghandi, Jill P. Mesirov and P. Tamayo (2015).
832 "The Molecular Signatures Database Hallmark Gene Set Collection." Cell Systems 1(6):
833 417-425.
834 Link, J. M., J. R. Eng, C. Pelz, K. MacPherson-Hawthorne, P. J. Worth, S. Sivagnanam, D. J.
835 Keith, S. Owen, E. M. Langer, A. Grossblatt-Wait, et al. (2025). "Ongoing replication stress
836 tolerance and clonal T cell responses distinguish liver and lung recurrence and outcomes
837 in pancreatic cancer." Nature Cancer.
838 Link, J. M., C. Pelz, P. J. Worth, S. Owen, D. Keith, E. M. Langer, A. Grossblatt-Wait, A. L.
839 Creason, J. Egger, H. Holly, et al. (2022). "Ongoing Replication Stress Response and New

840   Clonal T Cell Development Discriminate Between Liver and Lung Recurrence Sites and
841   Patient Outcomes in Pancreatic Ductal Adenocarcinoma." bioRxiv:
842   2022.2005.2004.490552.
843   Liu, Y. C., F. Li, J. Handler, C. R. Huang, Y. Xiang, N. Neretti, J. M. Sedivy, K. I. Zeller and C. V.
844   Dang (2008). "Global regulation of nucleotide biosynthetic genes by c-Myc." PLoS One **3**(7):
845   e2722.
846   Lourenco, C., D. Resetca, C. Redel, P. Lin, A. S. MacDonald, R. Ciaccio, T. M. G. Kenney, Y.
847   Wei, D. W. Andrews, M. Sunnerhagen, et al. (2021). "MYC protein interactors in gene
848   transcription and cancer." Nature Reviews Cancer **21**(9): 579-591.
849   Lourenco, C., D. Resetca, C. Redel, P. Lin, A. S. MacDonald, R. Ciaccio, T. M. G. Kenney, Y.
850   Wei, D. W. Andrews, M. Sunnerhagen, et al. (2021). "MYC protein interactors in gene
851   transcription and cancer." Nat Rev Cancer **21**(9): 579-591.
852   Luoto, K. R., A. X. Meng, A. R. Wasylishen, H. Zhao, C. L. Coackley, L. Z. Penn and R. G.
853   Bristow (2010). "Tumor cell kill by c-MYC depletion: role of MYC-regulated genes that
854   control DNA double-strand break repair." Cancer Res **70**(21): 8748-8759.
855   Lutterbach, B. and S. R. Hann (1994). "Hierarchical phosphorylation at N-terminal
856   transformation-sensitive sites in c-Myc protein is regulated by mitogens and in mitosis."
857   Mol Cell Biol **14**(8): 5510-5522.
858   Maere, S., K. Heymans and M. Kuiper (2005). "BiNGO: a Cytoscape plugin to assess
859   overrepresentation of gene ontology categories in biological networks." Bioinformatics
860   **21**(16): 3448-3449.
861   Murayama, T., Y. Takeuchi, K. Yamawaki, T. Natsume, M. Li, R. N. Marcela, T. Nishimura, Y.
862   Kogure, A. Nakata, K. Tominaga, et al. (2021). "MCM10 compensates for Myc-induced DNA
863   replication stress in breast cancer stem-like cells." Cancer Sci **112**(3): 1209-1224.
864   Papadopoulos, D., S. A. Ha, D. Fleischhauer, L. Uhl, T. J. Russell, I. Mikicic, K. Schneider, A.
865   Brem, O. R. Valanju, G. Cossa, et al. (2024). "The MYCN oncoprotein is an RNA-binding
866   accessory factor of the nuclear exosome targeting complex." Mol Cell **84**(11): 2070-
867   2086.e2020.
868   Papadopoulos, D., D. Solvie, A. Baluapuri, T. Endres, S. A. Ha, S. Herold, J. Kalb, C.
869   Giansanti, C. Schülein-Völk, C. P. Ade, et al. (2022). "MYCN recruits the nuclear exosome
870   complex to RNA polymerase II to prevent transcription-replication conflicts." Mol Cell **82**(1):
871   159-176.e112.
872   Petroni, M., F. Sardina, C. Heil, M. Sahún-Roncero, V. Colicchia, V. Veschi, S. Albini, D.
873   Fruci, B. Ricci, A. Soriani, et al. (2016). "The MRN complex is transcriptionally regulated by
874   MYCN during neural cell proliferation to control replication stress." Cell Death Differ **23**(2):
875   197-206.
876   Popov, N., M. Wanzel, M. Madiredjo, D. Zhang, R. Beijersbergen, R. Bernards, R. Moll, S. J.
877   Elledge and M. Eilers (2007). "The ubiquitin-specific protease USP28 is required for MYC
878   stability." Nat Cell Biol **9**(7): 765-774.
879   Queitsch, K., T. W. Moore, B. L. O'Connell, R. V. Nichols, J. L. Muschler, D. Keith, C. Lopez,
880   R. C. Sears, G. B. Mills, G. G. Yardımcı, et al. (2023). "Accessible high-throughput single-cell
881   whole-genome sequencing with paired chromatin accessibility." Cell Rep Methods **3**(11):
882   100625.

883   Robson, S. C., L. Ward, H. Brown, H. Turner, E. Hunter, S. Pelengaris and M. Khan (2011).
884   "Deciphering c-MYC-regulated genes in two distinct tissues." BMC Genomics **12**(1): 476.
885   Rohban, S., A. Cerutti, M. J. Morelli, F. d'Adda di Fagagna and S. Campaner (2017). "The
886   cohesin complex prevents Myc-induced replication stress." Cell Death & Disease **8**(7):
887   e2956-e2956.
888   Rousseau, V., E. Einig, C. Jin, J. Horn, M. Riebold, T. Poth, M.-A. Jarboui, M. Flentje and N.
889   Popov (2023). "Trim33 masks a non-transcriptional function of E2f4 in replication fork
890   progression." Nature Communications **14**(1): 5143.
891   Sears, R., F. Nuckolls, E. Haura, Y. Taya, K. Tamai and J. R. Nevins (2000). "Multiple Ras-
892   dependent phosphorylation pathways regulate Myc protein stability." Genes Dev **14**(19):
893   2501-2514.
894   Sears, R. C. (2004). "The life cycle of C-myc: from synthesis to degradation." Cell Cycle **3**(9):
895   1133-1137.
896   Shannon, P., A. Markiel, O. Ozier, N. S. Baliga, J. T. Wang, D. Ramage, N. Amin, B.
897   Schwikowski and T. Ideker (2003). "Cytoscape: a software environment for integrated
898   models of biomolecular interaction networks." Genome Res **13**(11): 2498-2504.
899   Solvie, D., A. Baluapuri, L. Uhl, D. Fleischhauer, T. Endres, D. Papadopoulos, A. Aziba, A.
900   Gaballa, I. Mikicic, E. Isaakova, et al. (2022). "MYC multimers shield stalled replication
901   forks from RNA polymerase." Nature **612**(7938): 148-155.
902   Stine, Z. E., Z. E. Walton, B. J. Altman, A. L. Hsieh and C. V. Dang (2015). "MYC, Metabolism,
903   and Cancer." Cancer Discov **5**(10): 1024-1039.
904   Stirling, D. R., M. J. Swain-Bowden, A. M. Lucas, A. E. Carpenter, B. A. Cimini and A.
905   Goodman (2021). "CellProfiler 4: improvements in speed, utility and usability." BMC
906   Bioinformatics **22**(1): 433.
907   Stringer, C., T. Wang, M. Michaelos and M. Pachitariu (2021). "Cellpose: a generalist
908   algorithm for cellular segmentation." Nat Methods **18**(1): 100-106.
909   Su, Y., C. Pelz, T. Huang, K. Torkenczy, X. Wang, A. Cherry, C. J. Daniel, J. Liang, X. Nan, M. S.
910   Dai, et al. (2018). "Post-translational modification localizes MYC to the nuclear pore basket
911   to regulate a subset of target genes involved in cellular responses to environmental
912   signals." Genes Dev **32**(21-22): 1398-1419.
913   Sun, X.-X., Y. Li, R. C. Sears and M.-S. Dai (2021). "Targeting the MYC Ubiquitination-
914   Proteasome Degradation Pathway for Cancer Therapy." Frontiers in Oncology **11**.
915   Tworkowski, K. A., A. A. Chakraborty, A. V. Samuelson, Y. R. Seger, M. Narita, G. J. Hannon,
916   S. W. Lowe and W. P. Tansey (2008). "Adenovirus E1A targets p400 to induce the cellular
917   oncoprotein Myc." Proc Natl Acad Sci U S A **105**(16): 6103-6108.
918   Tworkowski, K. A., S. E. Salghetti and W. P. Tansey (2002). "Stable and unstable pools of
919   Myc protein exist in human cells." Oncogene **21**(55): 8515-8520.
920   van Sluis, M. and B. McStay (2015). "A localized nucleolar DNA damage response facilitates
921   recruitment of the homology-directed repair machinery independent of cell cycle stage."
922   Genes Dev **29**(11): 1151-1163.
923   Vervoorts, J., J. Lüscher-Firzlaff and B. Lüscher (2006). "The ins and outs of MYC regulation
924   by posttranslational mechanisms." J Biol Chem **281**(46): 34725-34729.

925   Vesela, E., K. Chroma, Z. Turi and M. Mistrik (2017).
926   "Common Chemical Inductors of Replication Stress: Focus on Cell-Based Studies."
927   Biomolecules **7**(1).
928   Wang, Q., H. Zhang, K. Kajino and M. I. Greene (1998). "BRCA1 binds c-Myc and inhibits its
929   transcriptional and transforming activity in cells." Oncogene **17**(15): 1939-1948.
930   Welcker, M., A. Orian, J. E. Grim, R. N. Eisenman and B. E. Clurman (2004). "A nucleolar
931   isoform of the Fbw7 ubiquitin ligase regulates c-Myc and cell size." Curr Biol **14**(20): 1852-
932   1857.
933   Welcker, M., A. Orian, J. Jin, J. A. Grim, J. W. Harper, R. N. Eisenman and B. E. Clurman
934   (2004). "The Fbw7 tumor suppressor regulates glycogen synthase kinase 3
935   phosphorylation-dependent c-Myc protein degradation." Proceedings of the National
936   Academy of Sciences **101**(24): 9085-9090.
937   Wolf, F. A., P. Angerer and F. J. Theis (2018). "SCANPY: large-scale single-cell gene
938   expression data analysis." Genome Biol **19**(1): 15.
939   Wu, T., E. Hu, S. Xu, M. Chen, P. Guo, Z. Dai, T. Feng, L. Zhou, W. Tang, L. Zhan, et al. (2021).
940   "clusterProfiler 4.0: A universal enrichment tool for interpreting omics data." Innovation
941   (Camb) **2**(3): 100141.
942   Yeh, E., M. Cunningham, H. Arnold, D. Chasse, T. Monteith, G. Ivaldi, W. C. Hahn, P. T.
943   Stukenberg, S. Shenolikar, T. Uchida, et al. (2004). "A signalling pathway controlling c-Myc
944   degradation that impacts oncogenic transformation of human cells." Nature Cell Biology
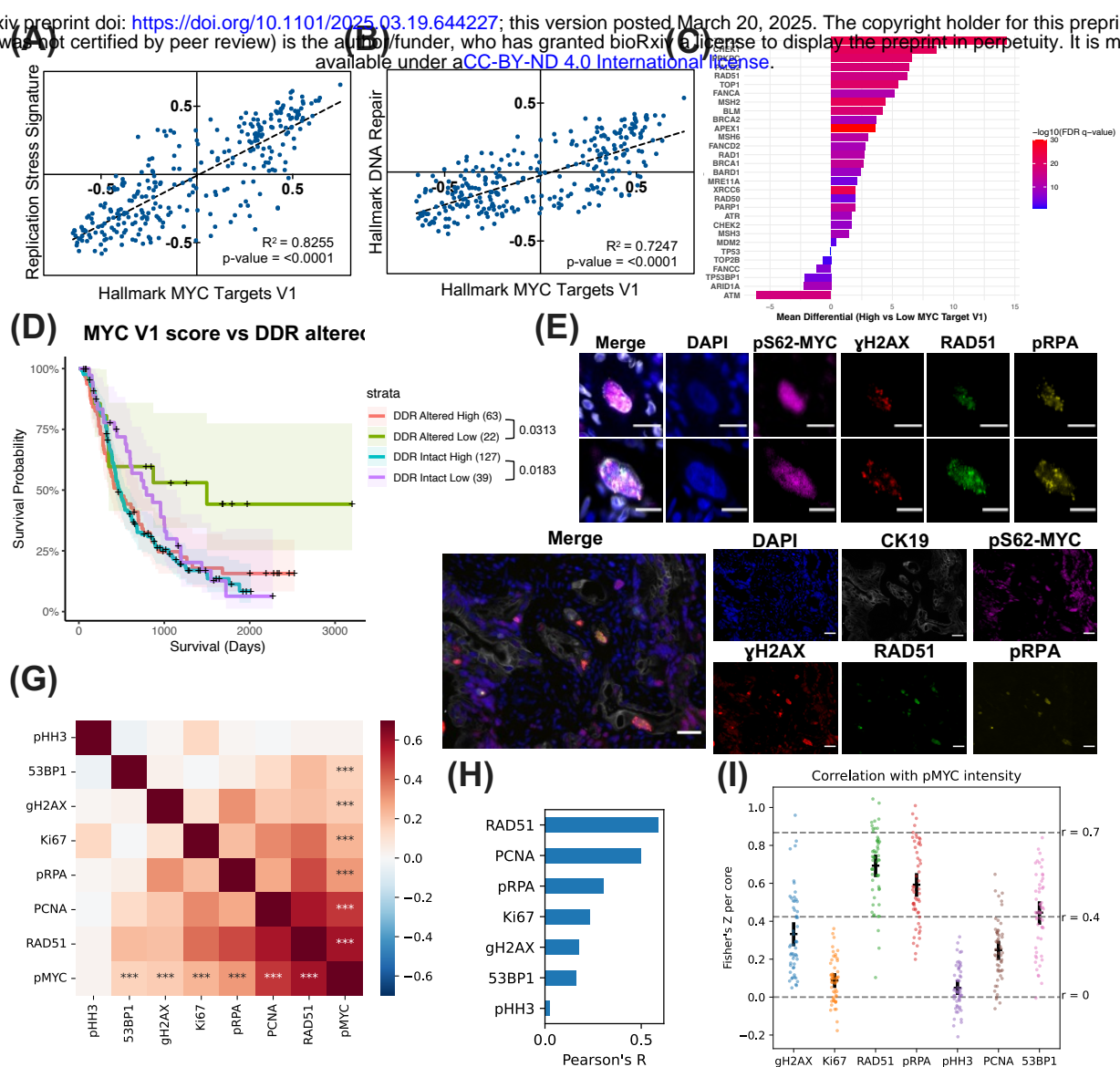945   **6**(4): 308-318.
946

Figure 1: MYC Activity Positively Correlates with Genomic Damage and Poor Patient Survival in PDAC. (A) Pearson correlations of RNA expression of 289 primary and metastatic PDAC tumors comparing GSVA scores of hallmark MYC-V1 targets and a replication stress gene signature (B) as well as hallmark DNA repair pathway. (C) Mean differential VIPER regulon activity for DNA maintenance factors between tumors with high or low hallmark MYC-V1 target score, with coloring indicating FDR q-values from a one-way ANOVA. (D) K-M graph of overall survival for patients with high or low hallmark MYC-V1 target score stratified by tumors with (DDR altered) or without (DDR intact) known somatic alterations in DNA damage response-related genes. Shaded regions represent 95% CI. All P-values not shown are greater than 0.05. (E) Two close-up images of pS62-MYC positive and DNA damage marker positive cells. Scale bar, 26μm. (F) Representative images of cyclic immunofluorescence analysis of a single core from a PDAC tissue microarray. Scale bar, 32.5μm. (G) Pearson correlation (two-sided) of mean antibody intensities (***)FDR <0.001. (H) Ranked Pearson's R correlation of mean antibody intensity. (I) Fisher's Z transformed Pearson correlation r value per core of single cell mean intensity correlation with pS62-MYC intensity for all 54 cores across 34 patients. Error bars represent the 95% confidence interval. Dotted lines represent Pearson r value of 0, 0.4 and 0.7, respectively.
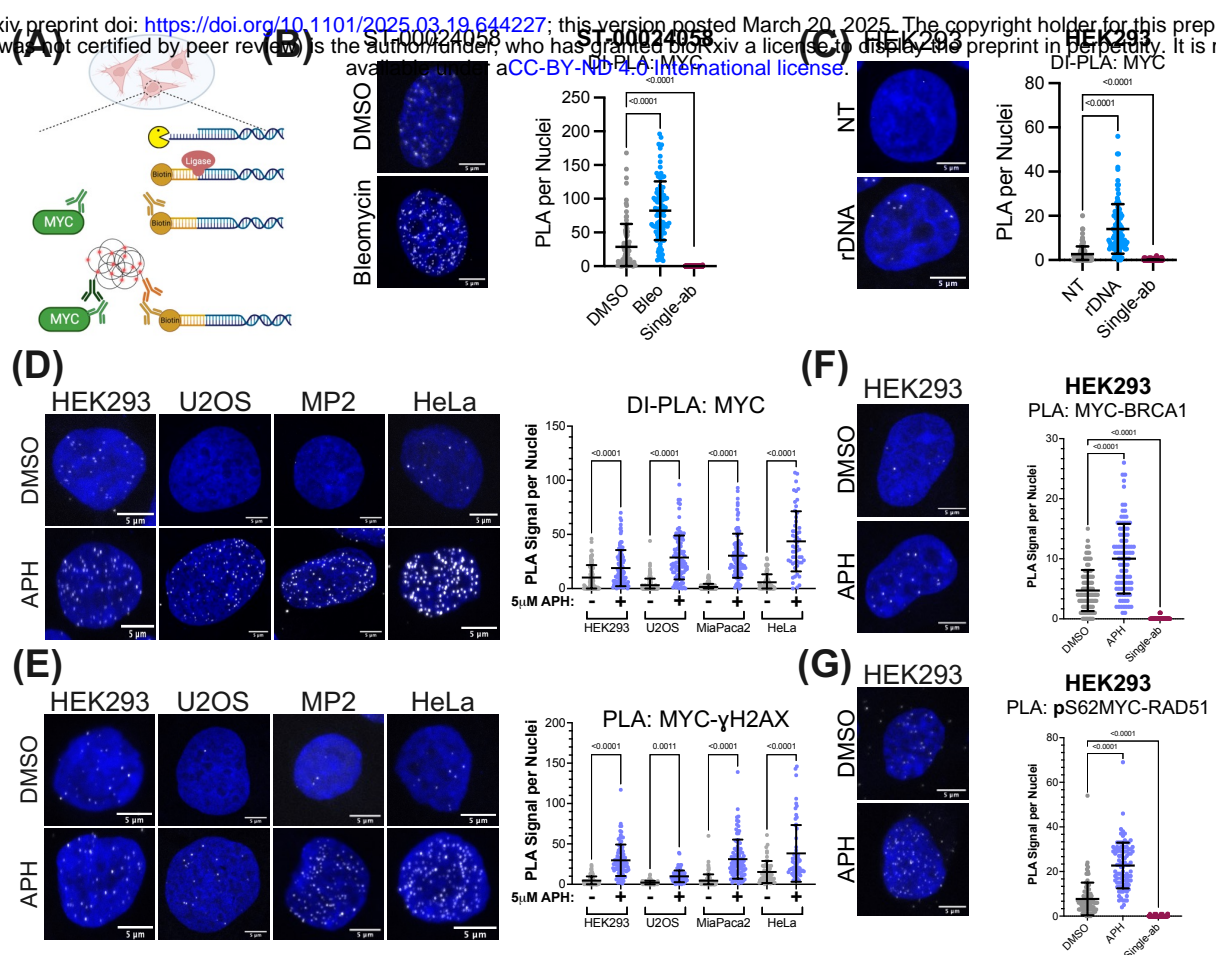
Figure 2: MYC is Detected in Proximity to DNA Double-Strand Breaks. (A) Schematic of DNA Damage in situ Proximity Ligation Assay (DI-PLA). (B) Left: Merged DI-PLA between MYC and biotin in a patient-derived PDAC cell line treated for 1 hour with 100 μg/mL bleomycin or DMSO. PLA puncta pseudo-colored in white. Right: quantification from three biological replicates of DI-PLA. Single antibody control combines PLA counts for both primary antibodies alone treated with bleomycin. The error bars show mean ±s.d. Statistical significance was determined by unpaired two-tailed t-test. (C) Left: Merged DI-PLA between MYC and biotin in HEK293 cells transfected with Cas9 protein and guide RNAs (sgRNA) targeting the 28S rDNA or non-targeting control (NT) for 8 hours. Right: quantification of DI-PLA. (D)Left: Representative images of DI-PLA between MYC and biotin in HEK293, U2OS, MIA PaCa-2, and HeLa cells treated with either 5μM APH or DMSO for 5-hours. PLA signal pseudo-colored in white. Left: Quantification of three biological replicates. (E) Left: Representative images of PLA between MYC and γH2AX. Right: Quantification of MYC and γH2AX PLA. (F) Left: Merged representative images of PLA between MYC and BRCA1 in HEK293 cells treated either DMSO or 5μM APH for 5-hours. Right: quantification of PLA. Single antibody control combines PLA counts for both primary antibodies alone treated with 5μM APH. (G) Left: PLA between pS62-MYC and RAD51 in HEK293 cells treated either DMSO or 5μM APH for 5-hours. Right: quantification of PLA. Note, MYC or pS62-MYC antibodies were chosen for PLA with RAD51 & BRCA1 antibodies based off cross-species compatibility.
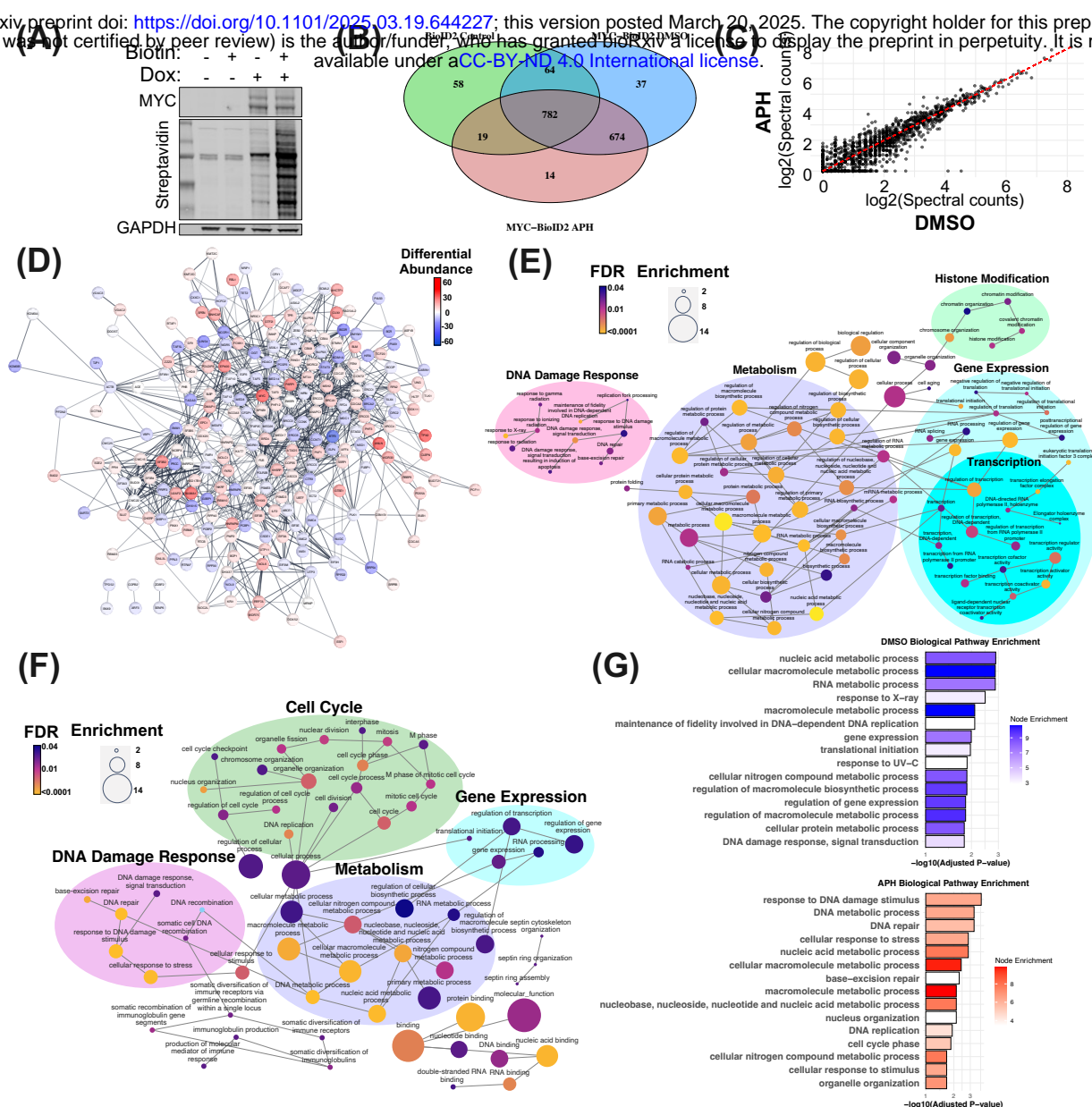
41

Figure 3: MYC Interactome is Enriched for DNA Repair Proteins Under Replication Stress. (A) Western Blot validation of inducible MYC-BioID2 construct in HEK293 cells treated with 1 μg/mL doxycycline for 24-hours and 50 μM biotin for 18-hours. (B) Venn diagram of biotinylated proteins detected in the different conditions, BioID2-only control (n=3), MYC-BioID2 treated with 24-hours of DMSO (n=3) or 5μM APH (n=2). (C) Scatter plot showing mean log2 value for the DMSO and APH conditions following background subtraction of BioID2-only. (D) Cytoscape interaction network analysis of MYC-BioID2 targets that pass a threshold of ≥2-fold differential abundance. Nodes colored based off mean spectral count differential abundance between APH (Red) and DMSO (Blue). BiNGO analysis showing the Gene Ontology (GO) enrichment network of DMSO (E) and APH (F). (G) Top 15 significantly enriched GO Biological pathway terms for DMSO (top) and APH (bottom).
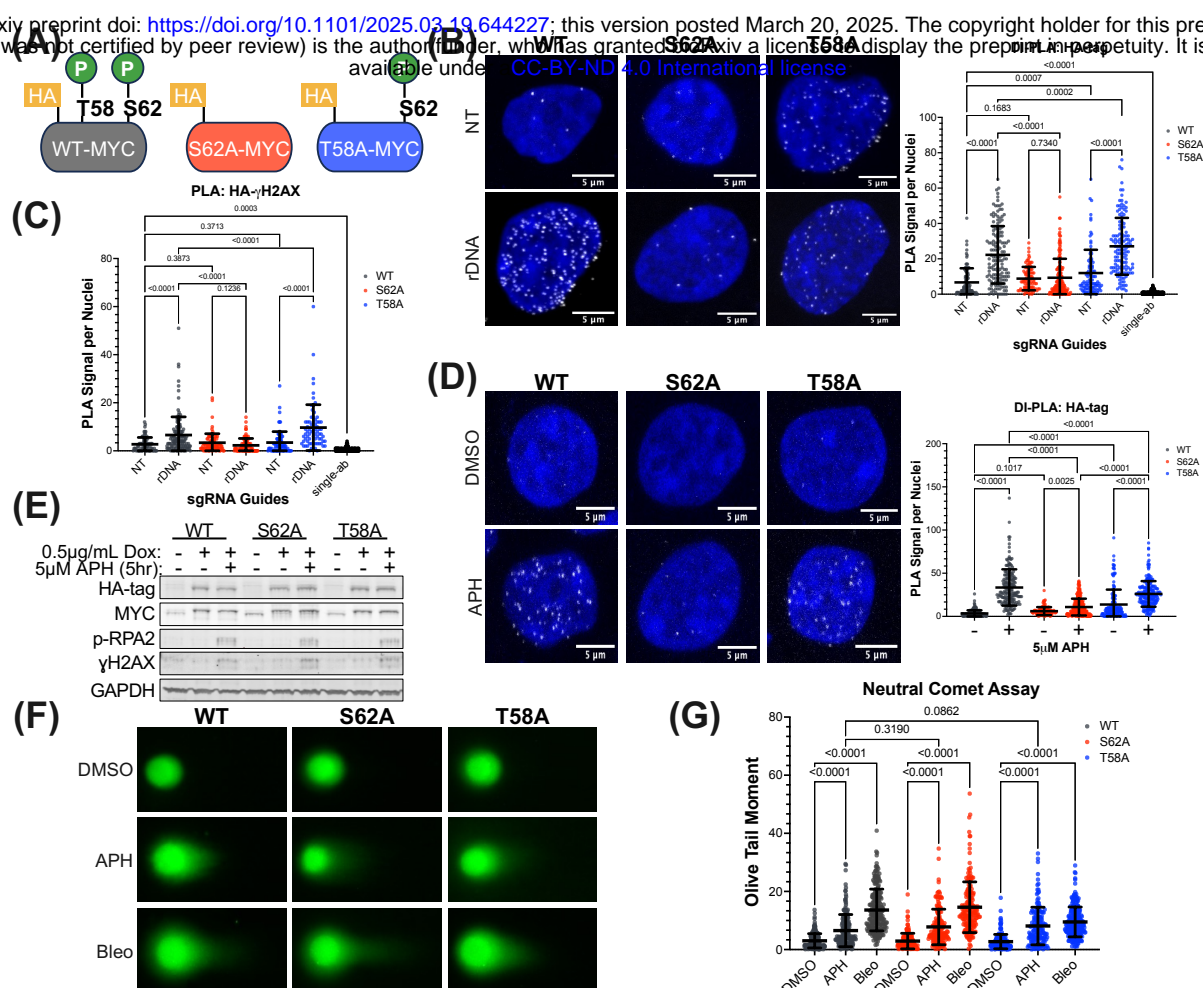
42

Figure 4: Serine 62 Phosphorylation of MYC Promotes its Association with DSBs.
(A) Schema of phosphorylation status of HA-tagged WT-MYC, S62A-MYC, and T58A-MYC in doxycycline inducible HEK293 cells. (B) *Left:* Merged DI-PLA between HA-tag and biotin treated for 18-hours with 0.5μg/mL doxycycline followed by an 8-hour transient transfection with Cas9 protein and guide RNAs (sgRNA) targeting the 28S rDNA or non-targeting control (NT). PLA puncta pseudo-colored in white. *Right:* Quantification of three biological replicates of DI-PLA in. Single antibody control combines PLA counts for both primary antibodies alone treated with rDNA guides. The error bars show mean ±s.d. Statistical significance was determined by ANOVA. (C) Quantification of three biological replicates of PLA between HA-tag and γH2AX. (D) *Left*: Merged representative single-cell images of DI-PLA between HA-tag and biotin treated for 18-hours with 0.5μg/mL doxycycline followed by 5μM APH (+) or DMSO (-) for 5 hours. Right: Quantification of three biological replicates with error bars showing mean ±s.d. and statistical significance was determined by ANOVA. (E) Western Blot analysis of WT-, S62A-, and T58A-MYC in HEK293 cell lines treated with 0.5μg/mL doxycycline for 18-hours followed by 5μM APH (+) or DMSO (-) for 5 hours. (F) Neutral comet assay following the same treatment as (E). 1-hour 100 μg/mL bleomycin treatment was positive control. (G) Quantification of (F) showing the Olive Tail Moment of three biological replicates. The error bars show mean ±s.d. Statistical significance was determined by ANOVA.

43

Figure 5: **Serine 62 Phosphorylation of MYC Regulates the Efficient Recruitment of BRCA1 and RAD51 to DSBs**. (A) Merged PLA between HA-tag and BRCA1 treated for 18-hours with 0.5μg/mL doxycycline followed by 5 hours of either DMSO or 5μM APH. PLA pseudo-colored in white. (B) Quantification of (A) experiment. Single antibody control combines PLA counts for both primary antibodies alone treated with 5μM APH for 5-hours. The error bars show mean ±s.d. Statistical significance was determined by ANOVA. (C) Merged PLA between HA-tag and RAD51 treated for 18-hours with 0.5μg/mL doxycycline followed by 5 hours of either DMSO or 5μM APH. PLA pseudo-colored in white. (D) quantification of (C). (E) Co-immunoprecipitation of transiently transfected Flag-tagged WT, T58A, or S62A-MYC in HEK293 cells followed by 5-hour treatment with either DMSO or 5μM APH. Anti-Flag antibody for precipitation followed by Western Blot analysis. (F) Merged DI-PLA experiment between BRCA1 and biotin in WT or S62A-MYC expressing HEK293 cells treated with 0.5μg/mL doxycycline for 18-hours followed by 5-hour treatment with either DMSO or 5μM APH. (G) Quantification of (F). (H) Merged DI-PLA experiment between RAD51 and biotin in WT or S62A-MYC expressing HEK293 cells treated with 0.5μg/mL doxycycline for 18-hours followed by 5-hour treatment with either DMSO or 5μM APH. (I) Quantification of (H).
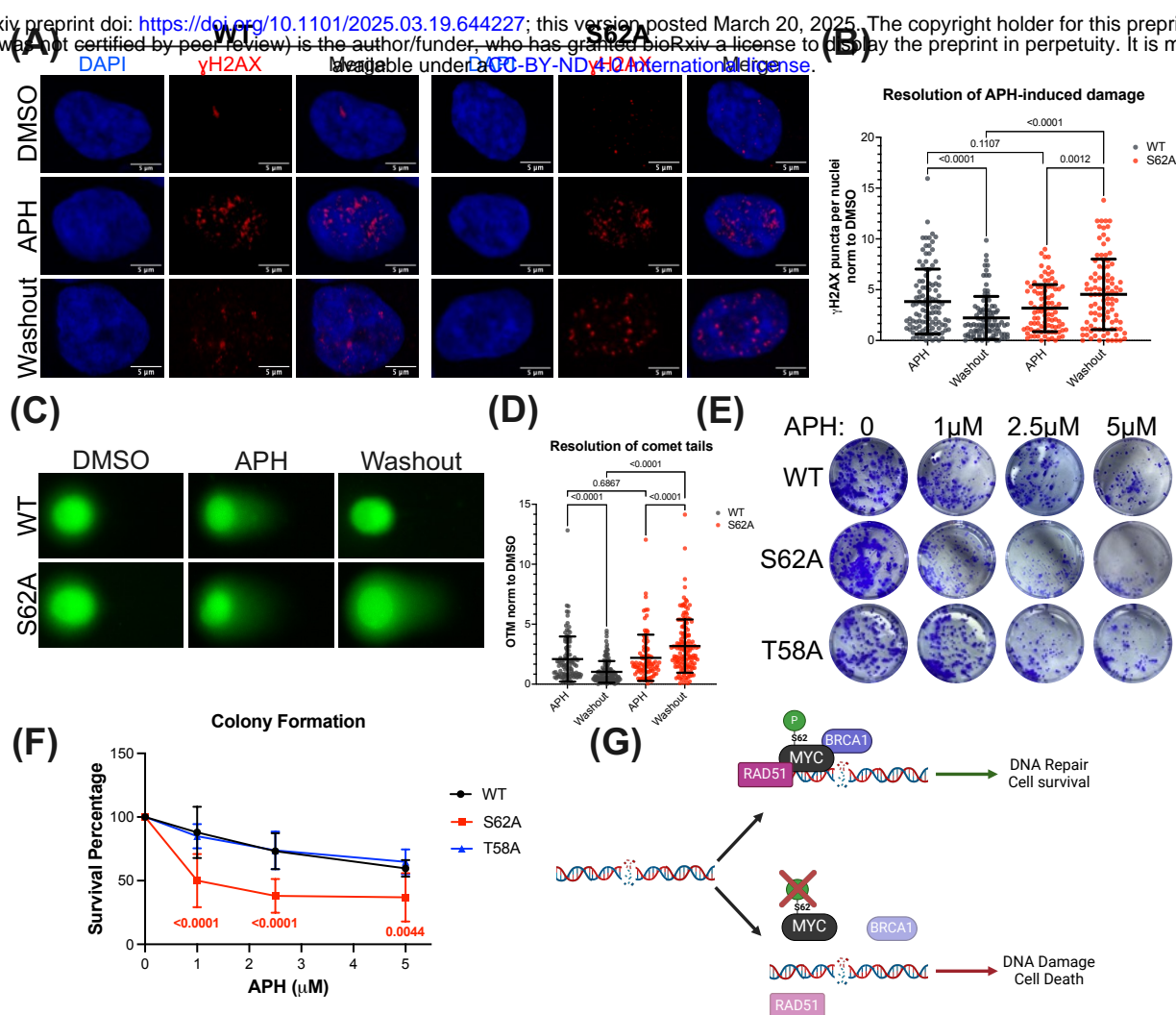
44

Figure 6: Phosphorylation of MYC at Serine 62 is Critical for DNA Damage Repair and Cell Survival in Response to APH-induced Stress. (A) Representative immunofluorescence images showing γH2AX puncta. WT- or S62A-MYC were induced by 18-hour 0.5μg/mL doxycycline treatment followed by either 5-hours of either DMSO or 5μM APH. Washout represents coverslips which were treated with 5μM APH for 5-hours followed by a media change with doxycycline for 3-hours. Statistical significance was determined by ANOVA. (B) Quantification of (A) comparing γH2AX puncta for 5-hour APH and 3-hour washout. Puncta were normalized to respective 5-hour DMSO or DMSO-washout condition. (C) Neutral comet assay of 3-hour washout post 5-hour DMSO or 5μM APH treatment in WT- or S62A-MYC HEK293 cells. (D) Quantification of (C) where washout APH treatment was normalized to washout DMSO. Statistical significance was determined by ANOVA. (E) 10-day Colony formation assay following 5-hour DMSO or APH in increasing concentrations. (F) Quantification of (E) showing the survival percentage of WT-, S62A-, and T58A-MYC expressing cells following 5-hour APH treatment. Statistical significance was determined by ANOVA. (G) Graphical summary of findings.

45